CHALMERS

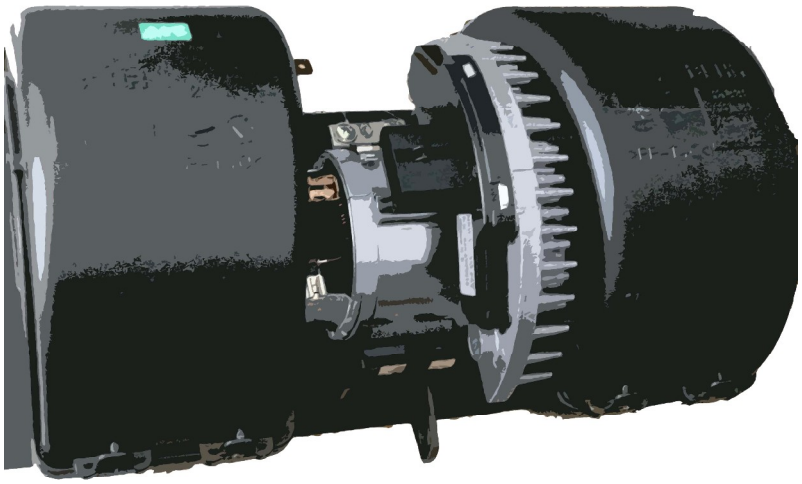

High efficiency actuators

Master of Science Thesis

Fredrik Andersson

Lars Karlsson

Department of Energy and Environment

Department of Signals and Systems

CHALMERS UNIVERSITY OF TECHNOLOGY

Göteborg, Sweden, 2007

Abstract

The permanent magnet direct current (PMDC) motor has been the most widely used actuator for vehicles due to its low price, high starting torque and easy control. The drawbacks are the relatively low efficiency and life length due to the carbon brushes used for commutation. Today the high demand on fuel efficiency and more electrical loads in a vehicle, forces the automotive industry too seek for more efficient alternatives.

This report considers the brushless permanent magnet (PM) motors that use electronical commutation with both sensor and sensor less operation as an alternative to the PMDC motor.

In a case study a PMDC motor operating a compartment fan in a truck is rebuilt to a brushless PM application. The measurements of the application and comparisons together with simulations in Matlab/Simulink for the two motors are used for another case study regarding fans in a modern coach. The saving in electrical power is estimated to an equivalent saving in diesel fuel.

The rebuilt truck compartment fan saves in average 50 W electrical power over the actual speed region. With some assumptions, this may be estimated to an equivalent savings of 70 liters of diesel annually for an average long haul truck.

The coach case study shows an annual saving of 700 liter diesel fuel by changing the electrical fan motor type from PMDC to a brushless PM.

It can be shown that the brushless PM motors benefits from higher efficiency and longer lifetime than the PMDC. Furthermore, the motor driver technology is of utmost importance for total efficiency.

Keywords: DC motor, PMDC, PMSM, BLDC, BLDC drivers, automotive actuators, high efficiency.

Acknowledgements

Bo Egardt	Chalmers / Department of Signals and Systems
Torbjörn Thiringer	Chalmers / Department of Energy and Environment
Johan Åström	Chalmers / Department of Energy and Environment
Sonja Tidblad Lundmark	Chalmers / Department of Energy and Environment
Mats Leksell	KTH / School of Electrical Engineering
Emma Jönsson	VTEC, group 6230
Eilert Johansson	VTEC, group 6230
Joachim Lindström	VTEC, group 6120
Michael Mankel	International Rectifier GmbH

Table of Content

List of symbols, subscripts and abbreviations

Symbols

A	slope
e	back EMF
θ	rotor angle
ω	rotor speed
g	gravity constant
I	current
T	torque
P	power
R_i	resistance interpole winding
R_r	rotor resistance
R_{brush}	PMDC brush resistance
K_e	emf constant
K_t	torque constant
Φ	phase
V	voltage
E	Absolute error
Z	magnitude

Subscripts

Ref	reference value
a, b, c	phase
B	beginning
e	electric
E	end
m	motor
s	switch
l	load

Abbreviations

AC	alternating current
ADC	analog to digital converter
DC	direct current
ECC	electronic climate control
PWM	pulse width modulation
BLDC	brushless direct current
EMF	electromotive force
EMC	electromagnetic compatibility
BEMF	back EMF
PM	permanent magnet
PMDC	permanent magnet DC
SR	switched reluctance
ECU	electronic control unit
CAN	controller area network
FOC	field oriented control
HVAC	heating, ventilation and air conditioning
ICE	internal combustion engine
VTEC	Volvo technology corporation

1. Introduction

Electrical actuators are an increasing part of the electrical power consumed in modern vehicles. The electrical power used in a vehicle is produced in the generator via the combustion engine. This master thesis aims at increasing the efficiency on the electrified actuators in order to reduce fuel consumption and CO_2 emissions by using brushless PM motors.

To be able to create a rotating magnetical field from a DC supply, the DC motors traditionally use mechanical commutation which still is used in the majority of the automotive electrical actuators.

The brushless commutation was made possible by the development of the power switching technology using semiconductors in the 1960´s. The absence of microprocessors forced these DC motors to operate with six step switching technology and analog electronics to handle the commutation. By the arrival of microprocessors in the 1980´s the industry began working towards the motor technology of today with PM motors operating at high efficiency in sensor less operation with both six step- and sinusoidal commutation, i.e. the applied stator voltage in the latter is the same as in the asynchronous motor. The PM motor driver of today is an embedded system with a microprocessor, PWM switching, ADC channels and a power stage consisting of the power semiconductor components. Due to the presence of cheap computer power, the state of the art in drive technology of today runs a brushless motor with sinusoidal commutation in sensor less operation using vector control. The processor also provides communication with other systems to add data feedback and robustness.

Global energy prices are at its all time high and the search for high efficiency motor drives are becoming more and more important in areas as in HVAC system that historically has been using asynchronous motors. This demand currently drives the development of the PM motors and their drives technology.

1.1 Purpose

The overall purpose with this project is to investigate if it is possible to save fuel in vehicles that use brushless PM motors as actuators instead of the brushed DC motor used today, and if so, how much fuel that can be saved.

1.2 Goal

To investigate the electrical motor market to find a suitable replacement for the DC motor and to rebuild the existing truck compartment fan with a high efficiency motor. How high efficiency can be reached with the brushless PM motors of today? Measurements shall underlie calculations to present power relations and efficiency for an existing and a rebuilt system.

To study the impact of the motor driver board for total efficiency. Investigate different types of drives and their effect on total efficiency.

To implement a mathematical model of the PMDC and BLDC system in Matlab/Simulink. The model should give usable results to provide an understanding of the functionality of the motors.

To present improvements, future work and some possible areas where the high efficiency motors may give new ideas for engineering in the automotive industry as well as to discuss limitations.

1.3 Delimitations

The simulations in this project apply to larger vehicles such as trucks/buses with 24V system voltage.

Environmental aspects limits to the calculations of fuel saving. The environmental impact of motor material choice and EMC will not be investigated.

Drive electronics will be discussed on a theoretical level for different types of motor control, but will not be built. The sensor less driver may not be optimized for its application.

In calculations of efficiency, the iron-and magnet losses will not be considered. Only one quadrant operation will be considered, even though the BLDC electronics uses four quadrant power electronics. Furthermore, the thermal design will not be investigated.

2. Theoretical background

The direct current, DC motor has historically been the most widely used actuator for automotives due to its low price, high starting torque and easy control. The drawback is a relative low efficiency and shorter life length due to the brushes. This chapter considers the DC motor and alternatives. Basically all the DC motors considered in this chapter could be driven both as a motor and a generator both clockwise and counterclockwise, i.e. in all four quadrants shown in *figure 2.1*.

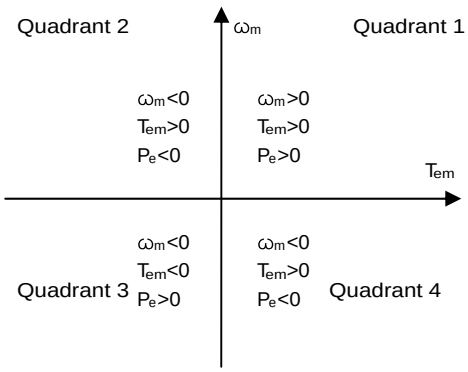

Figure 2.1: Quadrants requirement.

2.1 PMDC motor

The Permanent Magnet Direct Current, PMDC, motor has its magnetic field provided by permanent magnets in the stator and thus lacks the field windings from the shunt-/separately excited-/series- or compound DC motor. This yields no resistive losses in the field windings and improves total efficiency.

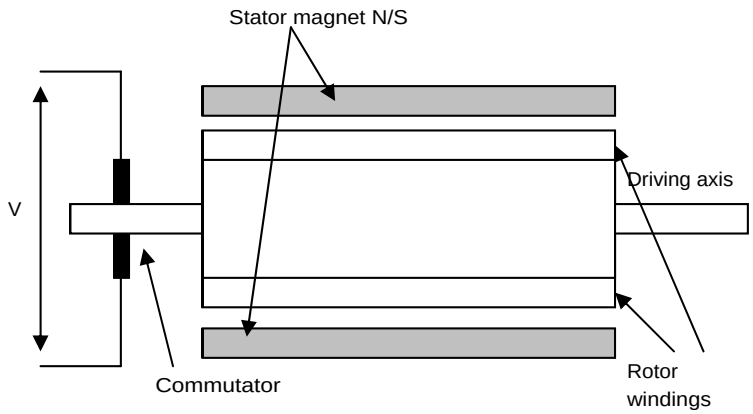

Figure 2.2: PMDC construction

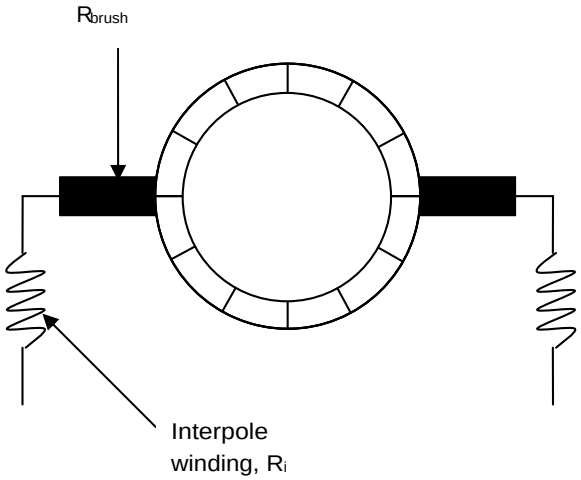

Figure 2.3: PMDC armature

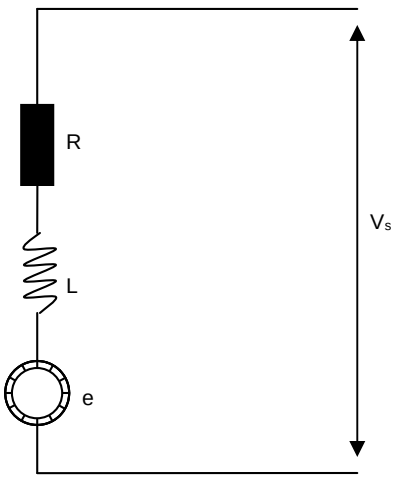

Figure 2.4: equivalent circuit

From the equivalent circuit in *figure 2.4* Ohms law yields

$$V_s = R\,i\ + L\frac{di}{dt} + e \tag{2.1}$$

where $R = R_{brush} + R_r + R_i$, and R_{brush} = brush resistance, R_r = rotor resistance and R_i = resistance interpole winding.

The rotation windings induce an electromotive force, e, and can be written as

$$e\ = K_e\omega \tag{2.2}$$

where ω denotes the speed in [rad/s]. The electric torque produced can be written as

$$T_e = K_t i \tag{2.3}$$

with K_e = emf constant and K_t = torque constant.

In a PMDC motor, the stator flux cannot vary and thus $K_t = K_e$ = constant.

Multiplying *(2.1)* with the armature current I at steady state ($\frac{dI}{dt} = 0$) gives the power balance:

$$V_s I = R\, I^2 + L\, I \frac{dI}{dt} + eI \Leftrightarrow P_{in} = P_{culosses} + P_{axle} \quad (2.4)$$

$$P_{axle} = T_{axle}\omega \quad (2.5)$$

$$\eta = \frac{P_{axle}}{P_{in}} \quad (2.6)$$

The lifetime is limited by the brushes that eventually will be worn out and needs replacement in 6-10 000 hours of operation. [5]

2.2 PMDC drives

The DC motor can be controlled by armature or field control. The PMDC has a constant flux via the permanent magnets so the only option is to control the armature.

The PMDC motor is speed controlled by varying its armature voltage and this can be implemented by PWM switching, i.e. a DC/DC converter, via a potentiometer or a transistor operating in the linear region. The two latter alternatives above give massive losses when driving at low speed. For instance, if a 24 V PMDC motor is to be driven at 8V, the transistor or the potentiometer has to lower the voltage with 16 V which will give massive losses. The advantage is that the problems with EMC will be kept at a minimum.

2.3 PMDC alternatives

There are some alternatives to the PMDC worth considering when aiming for high efficiency. The most important physical aspect is to get rid of the mechanical commutation using brushes. The voltage drop due to the brushes decreases efficiency. With the alternative of electronic commutation the losses can be kept at a minimum.

A small physical gap between the rotor and stator reduces magnetic air gap losses. The rotor core should be laminated with thin iron wafers to reduce eddy currents. It can be summed up that electronic commutation, no losses in the rotor due to windings and expensive manufacturing – thin iron wafers and a small air gap - is desirable for high efficiency.

This gives some alternatives considered below.

2.3.1 BLDC motor

The brushless direct current, BLDC, motor in *figure 2.5* has its permanent magnets on the rotor and can be seen as a PMDC motor turned inside out. The BLDC motor uses electronic commutation based on the position of the rotor in 60˚ interval and is considered as a highly efficient and robust motor. The motor is driven with two phases energized and the third left unconnected. This gives a trapezoidal waveform of the terminal voltage. The position can be supplied by hall sensors or by sensor less methods. There are problems with the starting torque at sensor less operation, see section *2.5.3.1 Start up strategies*, which makes it a good alternative when the starting torque is low, typically a fan or pump application.
The BEMF gives a trapezoidal waveform, since the magnets have a uniform shape, see *Figure 2.8.*

2.3.2 PMSM

The Permanent Magnet Synchronous Machine, PMSM, and the BLDC motors are basically the same motor, but the design of the rotor magnets differ. In the BLDC motor the magnets generate a trapezoidal BEMF but in the PMSM it generates a sinusoidal shape of the BEMF. Both motors share the same problem with the starting torque in sensor less mode.

The PMSM is fed with sinusoidal voltages which require the driver to know the position of the rotor with a high resolution. This was in the past accomplished by a high resolution encoder. Algorithms have been developed to run the PMSM in sensor less mode – by calculating its position with high accuracy. However, this feature requires more computer power and a start up technique to get measurable data. This PMSM start up algorithm is similar to the BLDC sensor less start up sequence in *section 2.5.3.1 Start up strategy.*

The sensor less PMSM driver measures on two phases and then applies field oriented control, FOC, to estimate rotor position. FOC is also known as vector control.

When comparing BLDC motors and PMSM some basic conclusions can be drawn. By assuming that the power factor for a PMSM is unity and that the copper losses is equal for both motors, calculation shows that the PMSM has 15% less power density than BLDC [1]. This is due to the different applied current shapes. This implies that a PMSM motor, for the same torque, must be made to handle larger peak currents. The advantage for the PMSM is lower torque ripple which gives higher efficiency [32].

2.3.3 SR motor

The switched reluctance motor is a simple machine using the phenomena that the magnetic field flows towards the lowest magnetic resistance path. The rotor is built up by an iron core and uses no magnets. The stator windings that provide the field are controlled with electronics and the rotor position needs to be known either by Hall sensors or sensor less driving. The SR motor is robust and cheap but the efficiency is considered lower than for the BLDC and PMSM. The SR motor is also known to produce torque variations, which may cause problems but most likely not for the fan application considered in this report.

This implies that the brushless PM motors are the most likely alternatives to replace the PMDC motors in automotive applications.

2.4 BLDC motor

A BLDC motor has two or three phase windings in discrete number of pairs in the stator. This report considers a 3 phase Y connected BLDC when a BLDC motor is mentioned.

Two phases are activated by the drive system at the same time while the third is unconnected – floating. As with the SR motor/PMSM the rotor position needs to be known for proper operation, i.e. for the drive to decide which phase to energize. The rotor position can be measured or estimated, the latter can be referred to as sensor less control.

The advantages are higher power density – due to no losses in the rotor - , high efficiency and long lifetime. The lifetime appears only to be limited by the bearings and the electronics and is considered as long as 25 000 hours of operation. [5]

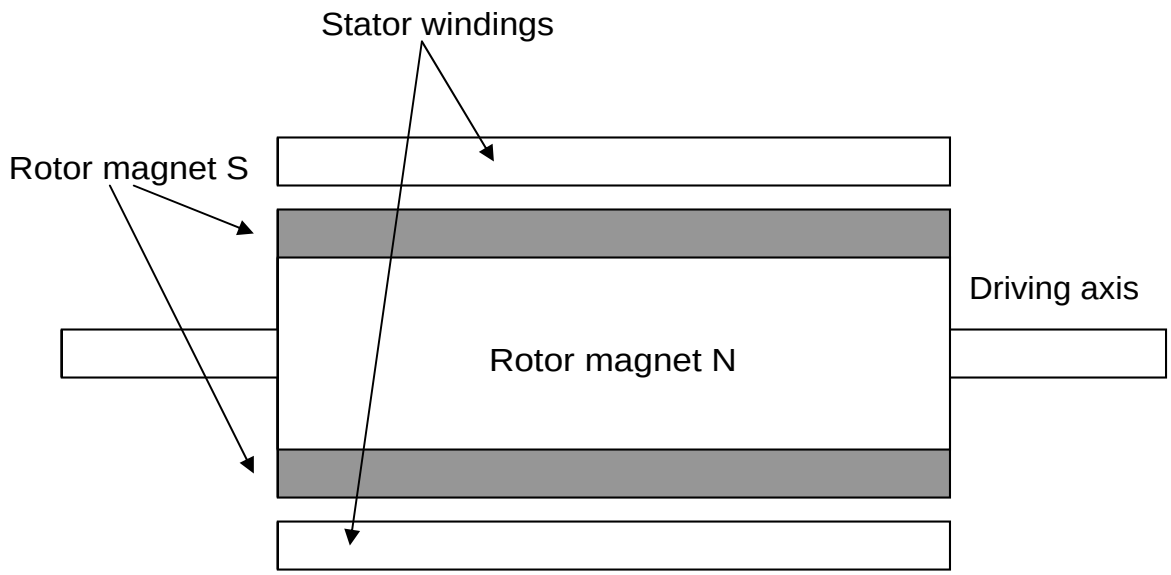

Figure 2.5 – basic principle BLDC

The three phases, star connected BLDC is represented by the following 4 equations:

$$v_{ab} = R(i_a - i_b) + L\frac{d}{dt}(i_a - i_b) + e_a - e_b \tag{2.7}$$

$$v_{bc} = R(i_b - i_c) + L\frac{d}{dt}(i_b - i_c) + e_b - e_c \tag{2.8}$$

$$v_{ca} = R(i_c - i_a) + L\frac{d}{dt}(i_c - i_a) + e_c - e_a \tag{2.9}$$

$$T_e = k_f\omega + J\frac{d\omega}{dt} + T_L \tag{2.10}$$

v, i and e denotes phase to phase voltage, phase current and phase BEMF, respectively in phase a, b and c. R and L are the stator resistance and inductance for each phase. T_L and T_e represent the load torque and the electric torque. J and k_f denotes the rotor inertia and friction constant, ω is the rotor speed.

According to the rotor position $\theta_m = \frac{p}{2}\theta_e$,where p denotes the numbers of poles, the BEMF can be expressed as follows.

$$e_a = \frac{k_e}{2}\omega \cdot F(\theta_e) \tag{2.11}$$

$$e_b = \frac{k_e}{2} \cdot \omega \cdot F\left(\theta_e - \frac{2\pi}{3}\right), \tag{2.12}$$

$$e_c = \frac{k_e}{2} \cdot \omega \cdot F\left(\theta_e - \frac{4\pi}{3}\right), \tag{2.13}$$

$$T_e = \frac{k_t}{2}\left[F(\theta_e)\cdot i_a + F\left(\theta_e - \frac{2\pi}{3}\right)\cdot i_b + F\left(\theta_e - \frac{4\pi}{3}\right)\cdot i_c\right] \tag{2.14}$$

The symbols k_t and k_e denotes the torque constant and the BEMF constant. The function $F(\theta_e)$ gives a trapezoidal waveform of the BEMF, see *figure 2.8: Ideal trapezoidal BEMF and corresponding activation voltages.*

2.5 BLDC drives

Information of the rotor position is essential for the BLDC drive to energize the correct stator winding. Incorrect energizing of phases leads to more torque variations, lowered lifetime and poor efficiency. The rotor position is determined by a position sensor or by measurements of the back EMF (sensor less). In sensor mode, a hall sensor provides this information and therefore the correct phase will be fired to start the motion of the rotor. The sensor less techniques are described further in section *2.5.3 Sensor less BLDC drive*.

The power electronics used are alike for the sensor and sensor less BLDC drive. Three full-bridges control the three phases in a four quadrant operation, as can be seen in *figure 2.6*.

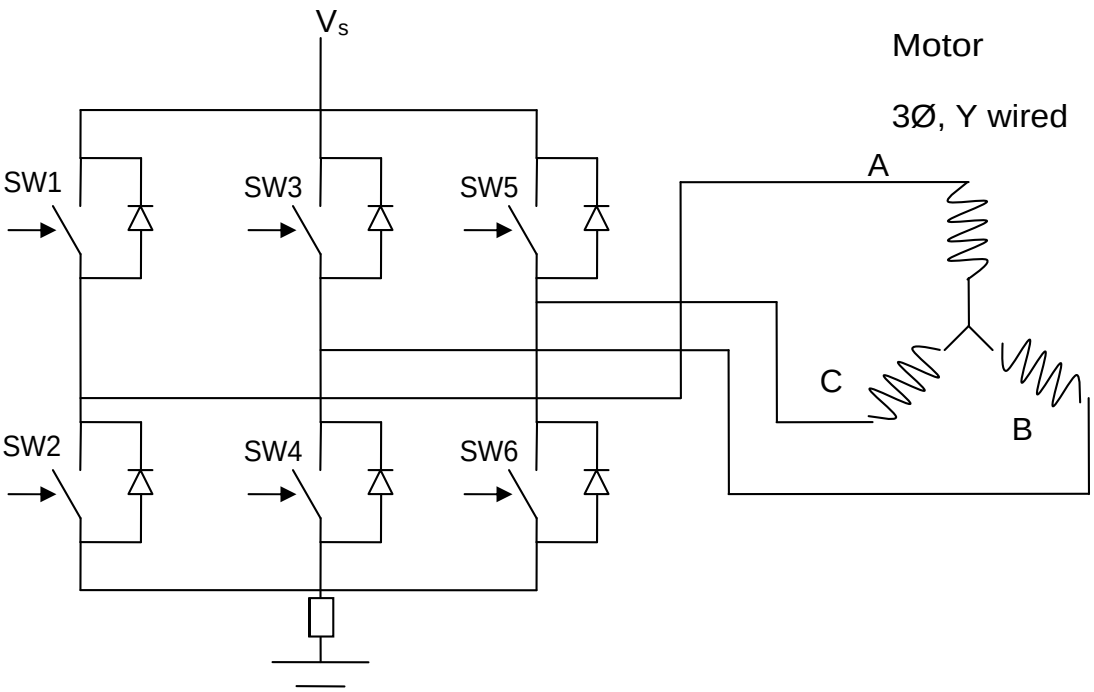

Figure 2.6: drive scheme BLDC

The freewheeling diodes seen in *figure 2.6*, shunt mounted across each switch, freewheels the currents when switching an inductive load and protects the transistor from the high voltage spikes that can occur.

The three switches connected to V_s are called high side switches and the three switches connected to ground are named low side switches. The single resistor between ground and the low side switches are used for current measuring purposes enabling an over current protection via an ADC to the controller. This resistor should be kept as low as possible to avoid losses but large enough to give ADC readings with sufficient accuracy.

As mentioned above two phases of the motor are always enabled and the third is left floating thus implying that there is always only one low- and one high side switch enabled at the same time.

If one phase winding is broken then the software controlling the power stage can implement a "*limp home*" mode where the motor is driven with reduced performance as a two phase motor with the broken phase left unconnected with floating voltage [8].

The gate driving circuits are controlled via pulse width modulation, PWM, to achieve the desired output voltage. Consider one switch in *figure 2.6* for explanation purposes. The duty rate, D, is defined as the part of one switch period when one transistor is conducting, thus $0 \leq D \leq 1$. A carrier wave, such as a saw tooth, sinus or triangular wave, and the desired output voltage is compared and the transistor is switched accordingly. This can be seen in *figure 2.7* below. By controlling the voltage to the three phases, the current can be controlled. The current gives a torque, as can be seen in *(2.14)*, and the applied electrical torque impacts the speed as in *(2.10)*.

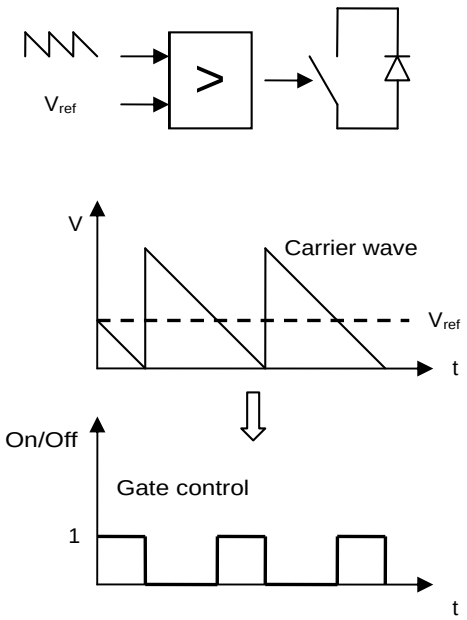

Figure 2.7: Saw tooth carrier wave in PWM switching.

2.5.2 Sensor driven BLDC

In a sensor driven BLDC three hall sensors (A, B, C) are used to supply the microcontroller with the rotor position. The hall sensors are mounted separately 120° from each other. By simultaneously using the information from each hall sensor, the rotor position can be defined within 60 degrees and hence commute the proper stator winding, see *table 2.1*. The advantages from this rotor positioning system are that the rotor position is always known, independent of the speed of the motor. The disadvantage of this technique is that the sensors and its copper wiring add to the total cost of the system and also increase the level of failure to the system. Furthermore, the hall elements need to be mounted in a high accuracy to achieve correct commutation, a misplaced hall sensor lowers total efficiency. Due to the actual knowledge of rotor position there is no problem with the starting torque as could be the case with sensor less operation, see below.

Table 2.1: Hall sensor value and corresponding commuted phase in clockwise rotation of the rotor.

Hall Sensor Value (CBA)	**Phase**	**Switches**
101	A-B	SW1;SW4
001	A-C	SW1;SW6
011	B-C	SW3;SW6
010	B-A	SW3;SW2
110	C-A	SW5;SW2
100	C-B	SW5;SW4

2.5.3 Sensor less BLDC drive

When a rotor magnet passes the floating phase in a BLDC motor, a voltage is induced. A sensor less BLDC drive measures this induced voltage, the BEMF, and calculates the corresponding rotor position in a microcontroller. The BEMF voltages in each phase to phase winding are measured by three Analog to Digital Converters, ADC´s. The microcontroller recognizes when the BEMF passes the zero crossing level and controls the gates of the power stage accordingly. With the power stage implied in *figure 2.6,* the zero crossing level is half the motor supply voltage V_s. One method is to have a signal connected from external comparators that fires a signal when the BEMF passes the zero crossing level.

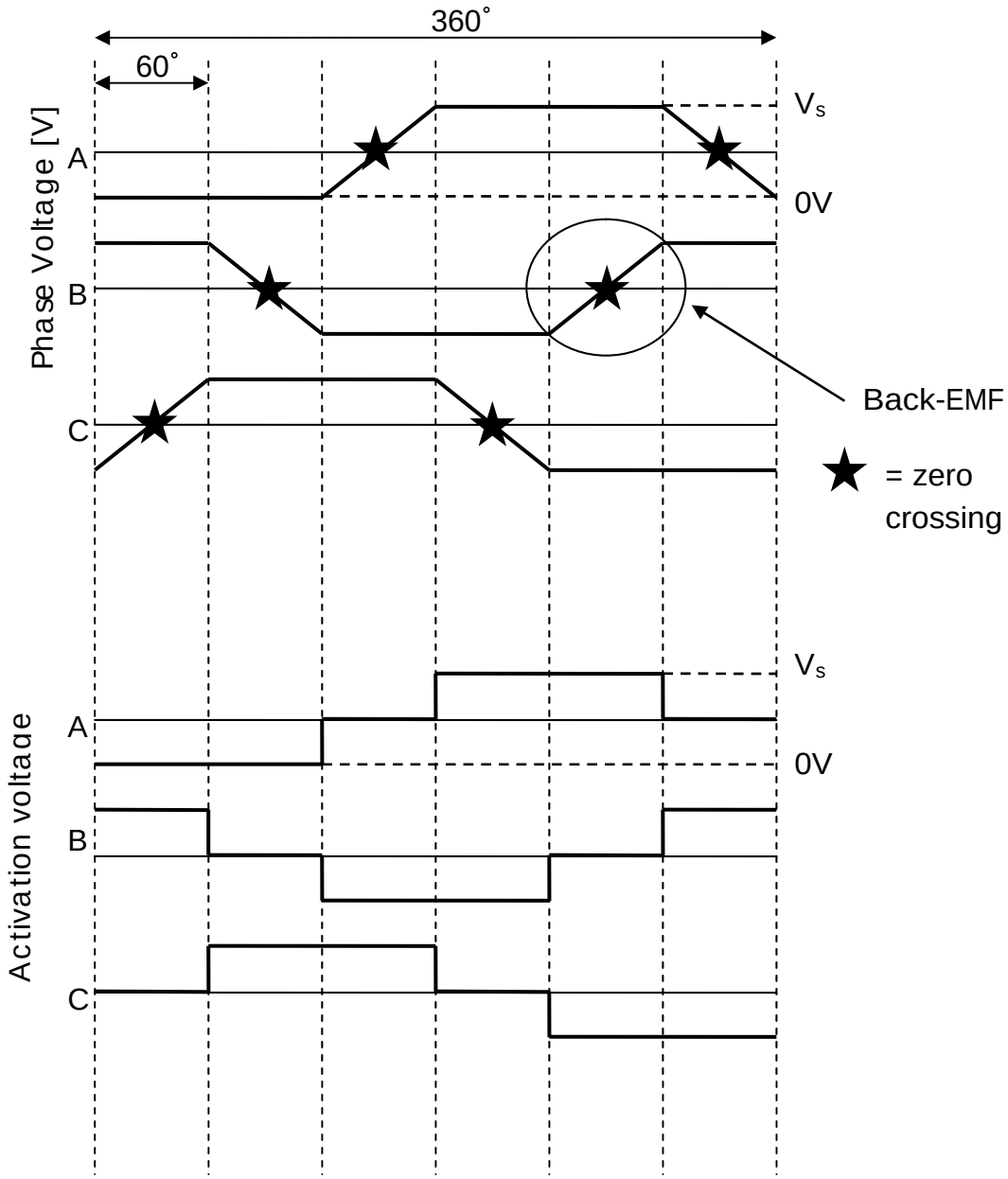

Figure 2.8: Ideal trapezoidal BEMF and corresponding activation voltages with low side to ground.

As can be seen in *figure 2.8* the optimal phase activation is ideally 30˚ after a zero crossing of the BEMF when the rotor is in correct position. Activating a phase too early or too late will give higher currents, torque counteracting the rotation of the rotor and poor efficiency. Misfiring of the phases will eventually break the motor. The dynamic speed interval where it is not possible to run sensor less is estimated to less than 5 % of maximum speed [32].

2.5.3.1 Start up strategy

At startup or standstill there is no BEMF to measure because the magnitude of the BEMF is directly proportional to the motor speed. This is a problem during start up and at low speeds when the signal to noise ratio for the ADC or comparator sensing the BEMF is too small, which makes the zero crossing impossible to detect. For this reason all sensor less BLDC drives needs a startup sequence before the sensor less algorithm is able to step in and take over the commutation of the motor. For how long time, and at which rpm, the startup sequence ends and an accurate zero crossing is possible to measure, varies for different motors and needs to be tuned in for each application [15] [19].

Inductance measuring

A method of aligning the rotor before commutation starts uses measurement of motor inductance, which makes the software independent regarding the choice of BLDC motor, load etc. The method uses variable inductance to detect initial rotor position. By an applied voltage over one phase, putting the other two phases to ground, a magnetic field is created. Then the other two phases are energized and the first phase is held to ground, creating an opposite magnetic field. The peak currents of the two opposing magnetic fields are then measured and compared. The largest peak will indicate the current that is in the same direction as the magnetic field caused by the rotor. The north pole of the rotor is found within 180˚. By repeating the entire procedure for the other two phases the north pole of the rotor can be sensed down to 60˚ which is enough for proper commutation [17].

Force drive

One way of creating the BEMF is to let the startup algorithm commutate the stator windings blindly, phase after phase until there is a possibility to measure the BEMF. At low speeds, there is a high possibility of detecting a zero crossing in another point than the ideally halfway through the 60˚ sector. This is due to a shallow slope of the BEMF; see *figure 2.9* compared to high-speed BEMF. Noise is also a powerful factor that makes it harder to detect the shallow slope. These problems result in premature zero crossing and thus, also premature commutation of the stator windings. By looking at the BEMF at the three phases respectively, the sensor less algorithm can analyze and recover in the following sectors by adjusting the commutation, increase the speed of the rotor and hence detect a more accurate BEMF. This method depends on inertia, BEMF-constant, torque constant, applied voltage and initial load, which make the startup algorithm sensitive for different BLDC motors and its application areas. Thus changing motor and application area needs updated software. An abrupt load torque at low speed can lock the rotor and make the start up impossible. Thus, this technique is mostly suitable for applications with low starting torque such as a fan or pump [15] [19].

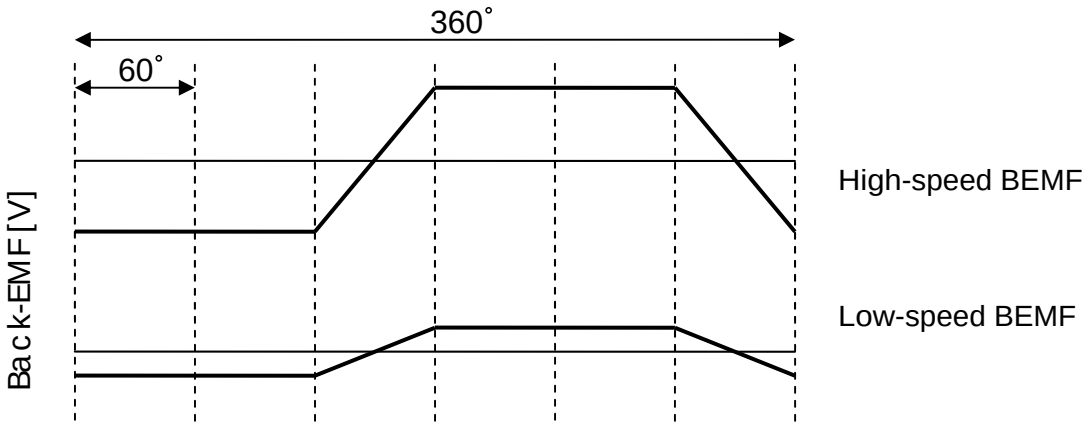

Figure 2.9: Ideal BEMF at high and low speed.

2.5.4 Optimal commutation

Regardless if the driving technique is sensor or sensor less there is always a risk of suboptimal commutation. In the sensor based system a mounting offset error in the hall elements increases with the multiplying of the pole pairs. In the sensor less system, measuring and filtering are used as instruments for computing commutation time and this technique is sensitive to measurement errors. Both methods may give suboptimal commutation which involves reduction of maximum torque and efficiency.

One proposed method in sensor less operation, to determine correct commutation time is to measure the terminal voltage of the energized winding at the beginning, V_{BF} and at the end, V_{EF} of a commutation period. A proper commutation implies that $V_{BF} = V_{EF}$, and a symmetric shape of the commutation is attained. By comparing V_{BF} and V_{EF}, the shape of the terminal voltage is shown to be asymmetric and that $V_{BF} \neq V_{EF}$. This commutation provides phase currents displayed in *figure 2.10a*. Compared to the proposed method displayed in *figure 2.10b* [24].

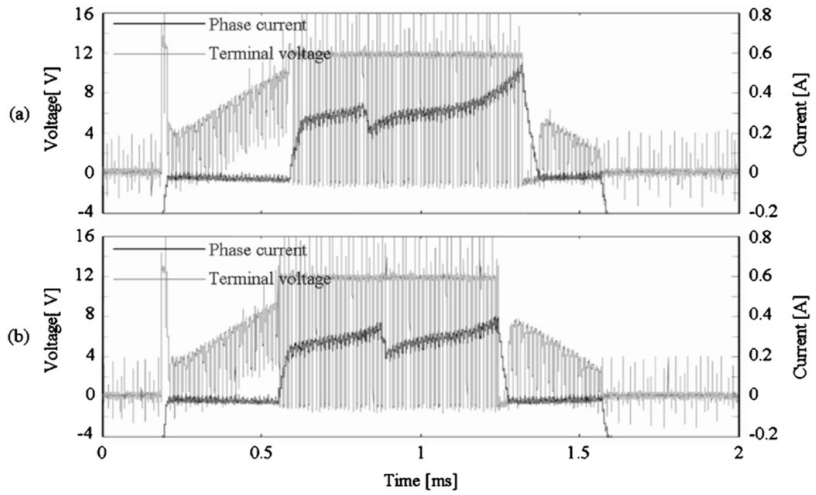

Figure 2.10: Terminal voltage and phase current. (a) Conventional method. (b) Proposed method .Courtesy of [24].

To measure the terminal voltage, access to the neutral point from the machine is needed. This can be achieved by one cable from the motor or by creating a virtual zero by connecting each phase to a resistor in Y connection.

The terminal voltage is filtered, as can be seen in *figure 2.11*, before measurements can be done. At a time window near the zero crossing point, not affected by the freewheeling currents and distorting noise, the BEMF voltage is linear and the measurements of T, Z and A can be done. Here T, Z, A denotes the shift angle, magnitude and slope of the filtered terminal voltage at the zero crossing position. The subscripts B and E denote beginning and end, respectively.

$$V_{BF} = A_B T_B + Z_B \tag{2.15}$$

$$V_{EF} = A_E T_E + Z_E \tag{2.16}$$

After averaging the measured values, for N number of mechanical revolutions, V_{BF} and V_{EF} are compared. If not equal, the microprocessor shifts the lead angle.

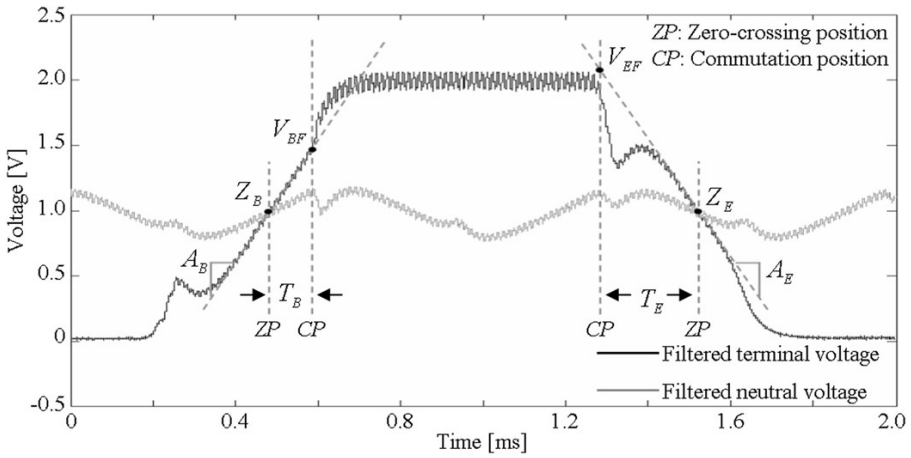

Figure 2.11: Filtered terminal voltage. Courtesy of [24].

An algorithm, see *figure 2.12*, can be implemented in software that computes the right values for these variables mentioned above, i.e. that V_{BF} becomes equal to V_{EF} according to *(2.15)* and *(2.16)*.

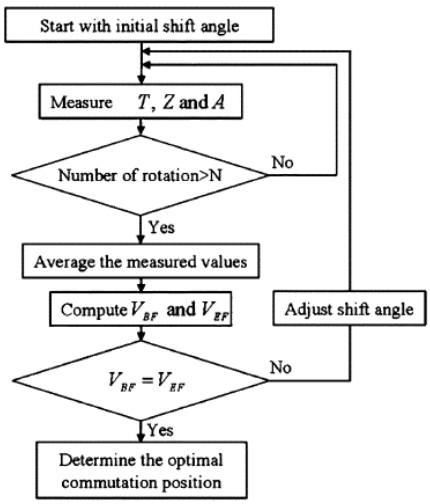

Figure 2.12: Algorithm of the proposed method. Courtesy of [24].

Research in this area, for one motor, has shown that a correct commutation will result in an increased efficiency up to 5% at full speed [24]. This method can also be applied to hall sensor based systems due to mounting offsets in the hall elements.

2.5.5 Electronic losses

Efficiency losses in the electronic circuitry are drawn from the low voltage electronics, as the microprocessor, and the power electronic parts. Compared to the power electronics, the losses in the low voltage electronics are considered negligible. The power electronics constitute semiconductors as diodes and transistors which are used as switching components. There are two types of losses from the switching components, conduction losses which originate from on-state operation and switching losses which result from turn-on and turn-off transitions [2].

2.5.5.1 On-state losses

Conduction losses are due to the transistor voltage drop generated by the conducting current as the switch is in its on-state mode. The voltage drop over the transistor consists of a constant voltage drop V_0 and the resistive voltage drop due to R_{on}.

$$V_{on} = V_0 + R_{on} I_{on} \tag{2.17}$$

here V_{on} denotes the total voltage drop and I_{on} denotes the current flowing through the switch at on-state. R_{on} is given by the transistor bias, i.e. if the transistor is operating in the linear area or the saturated area, see *figure 2.13*.

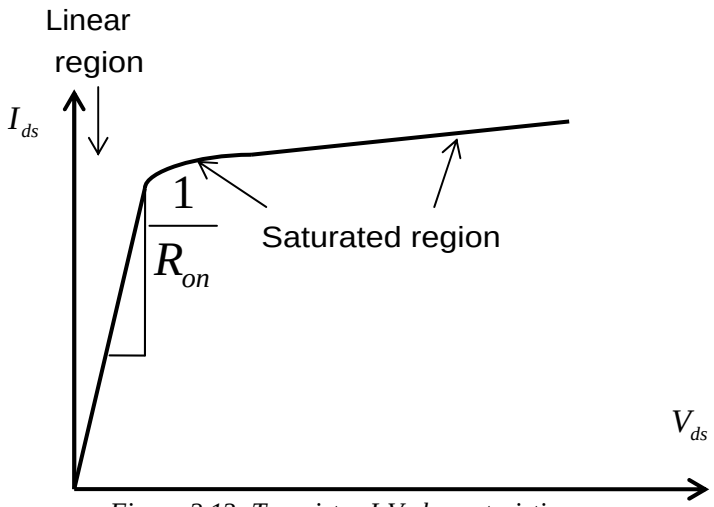

Figure 2.13: Transistor I-V characteristic

The energy dissipation W_{on} in the switch during on-state is approximated as

$$W_{on} = V_{on} I_{on} t_{on} \tag{2.18}$$

where t_{on} denote the on-state interval.

2.5.5.2 Switching losses

The switching losses increase with higher switching frequency. As voltage drop decays to V_{on} over the transistor and the current I_{on} starts to flow through the transistor the instantaneous switch energy loss is

$$W_{c(on)} = \frac{1}{2} V_{ds} I_{on} t_{c(on)} . \tag{2.19}$$

During turn-off I_{on} decays and the voltage over the transistor is increasing. The switch energy loss is expressed by

$$W_{c(off)} = \frac{1}{2} V_{ds} I_{on} t_{c(off)} \tag{2.20}$$

where $t_{c(on)}$ and $t_{c(off)}$ is the turn-on and turn-off interval. Switching losses are shown in *figure 2.14.*

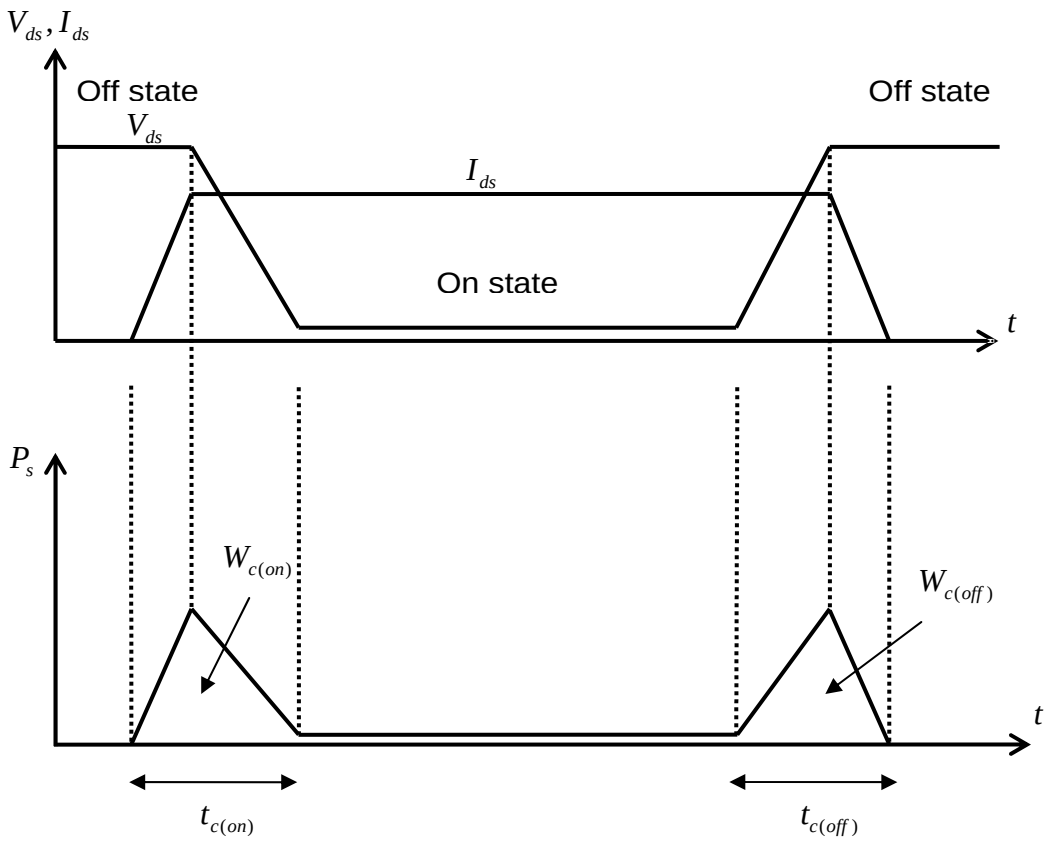

Figure 2.14: Scheme for determining switching losses

2.5.5.3 Total Power loss

The total power loss can be calculated by using *(2.18)* - *(2.20)* and convert them from energy to power by dividing with time

$$P_{on} = V_{on} I_{on} \frac{t_{on}}{T_s} \tag{2.21}$$

$$P_s = \frac{1}{2} V_d I_{on} f_s \left(t_{c(on)} + t_{c(off)} \right). \tag{2.22}$$

Combining *(2.21)* and *(2.22)* gives the total power loss

$$P_{tot} = P_{on} + P_s . \tag{2.23}$$

By turning on or off the switches when either the current or voltage is close to zero, it is possible to reduce the switching power losses and switching stresses.

3. Implementation

The existing BEHR truck compartment fan can be seen in *figure 3.1* and is driven by a 24V PMDC motor provided by BOSCH [9]. The PMDC drive is constructed as a class A amplifier, i.e. two parallel mounted transistors operated in their linear region. The gates of the transistors are controlled by electronics that respond to a 0-10V control signal from the ECC control unit. The driver heat dissipation is provided by the cooling unit.

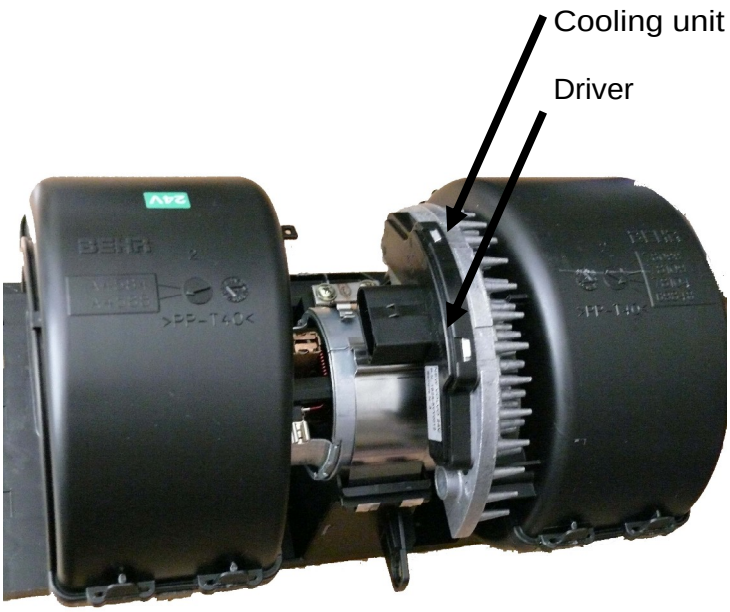

Figure 3.1: BEHR 24V compartment fan

Figure 3.2 displays a detailed view of the existing DC-motor.

Figure 3.2: BOSCH 24V DC-motor

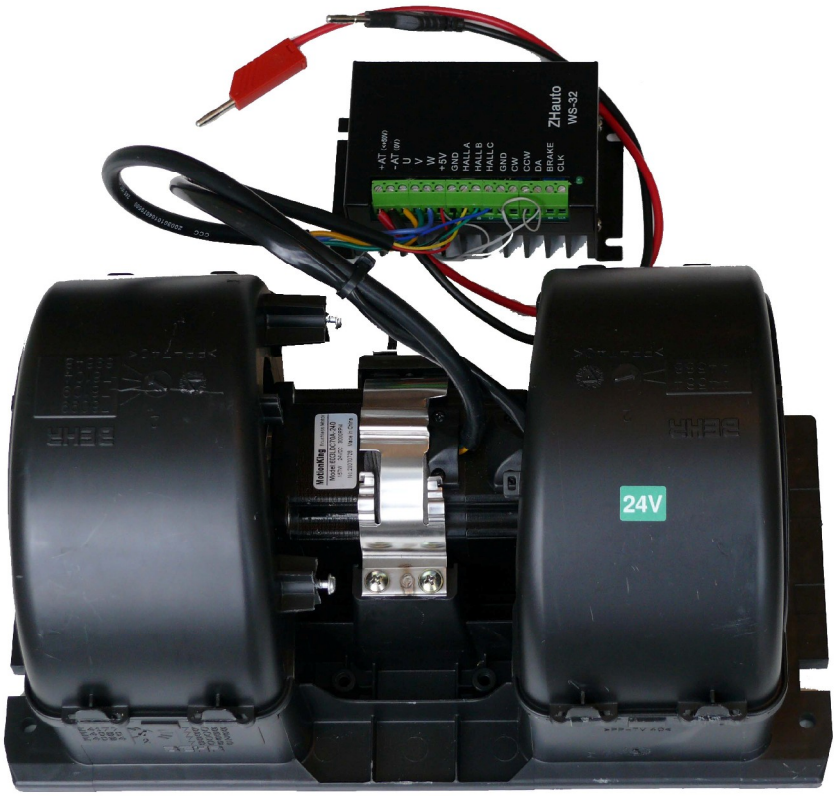

Figure 3.3: BEHR 24V compartment fan with power electronic and corresponding BLDC-motor

Figure 3.3 demonstrates the rebuilt compartment fan. The existing DC motor is replaced with a BLDC motor with hall sensors and its corresponding six step commutation driver. Also note that the mounted cooling unit in figure 3.1 is removed. *Figure 3.4* demonstrates a detailed view of the proposed BLDC motor.

F*igure 3.4: Motion King 24V BLDC-motor*

Table 3.1: Motor data

	BOSCH	**Motion King**
Type	PMDC	BLDC
Driver	Linear amplifier	PWM using Hall sensor
Voltage	26V	24V
Rated power	180 W	157 W
Rated speed	4300rpm	3000 rpm
Torque @ rated speed	0.4Nm	0.5Nm
Rated current	12.5 A	8.72 A
K_e	0.0495 (measured)	0.04 (measured)
K_t	= K_e	0.055 (measured)
Efficiency, stated	-	70-75%
Temperature interval	-20 to +50C	-20 to +50 C

Table 3.1 gives motor data of the existing and the replacing motor. Finding the same rating for two different motors is difficult, therefore the speed range must be taken into consideration. With these two motors, the level of load from each motor in the actual rpm region is comparable. The motor parameters were measured and then adjusted for the machine model. The main interest of the modeling is the efficiency and not the dynamic response, i.e. the moment of inertia was assumed to be small. The actual rpm region for comparisons is 650-3150 rpm. According to the BLDC manufacturer the magnets should cope with temperatures up to 180 ˚C without loosing their flux.

3.1 Modeling PMDC motor

A state-space model has been derived from equations presented in section *2.1 PMDC* and the complete state space model is expressed as equation *(3.1)* and *(3.2)*

$$\frac{d}{dt}\begin{pmatrix} i \\ \omega \\ \theta \end{pmatrix} = \begin{pmatrix} -\frac{R}{L} & -\frac{k_e}{L} & 0 \\ \frac{k_t}{J} & -\frac{k_f}{J} & 0 \\ 0 & 1 & 0 \end{pmatrix} \cdot \begin{pmatrix} i \\ \omega \\ \theta \end{pmatrix} + \begin{pmatrix} \frac{1}{L} & 0 \\ 0 & -\frac{1}{J} \\ 0 & 0 \end{pmatrix} \cdot \begin{pmatrix} V_s \\ T_L \end{pmatrix} \tag{3.1}$$

$$\begin{pmatrix} i \\ \omega \\ \theta \\ T_e \end{pmatrix} = \begin{pmatrix} 1 & 0 & 0 \\ 0 & 1 & 0 \\ 0 & 0 & 1 \\ k_t & 0 & 0 \end{pmatrix} \cdot \begin{pmatrix} i \\ \omega \\ \theta \end{pmatrix}. \tag{3.2}$$

The Matlab/Simulink implementation of the PMDC model consists of the state space model expressed by *(3.1)* and *(3.2)* and an efficiency calculation block, where the power of the driver circuit is added to the PMDC power and total efficiency is calculated, see *figure 3.5*.

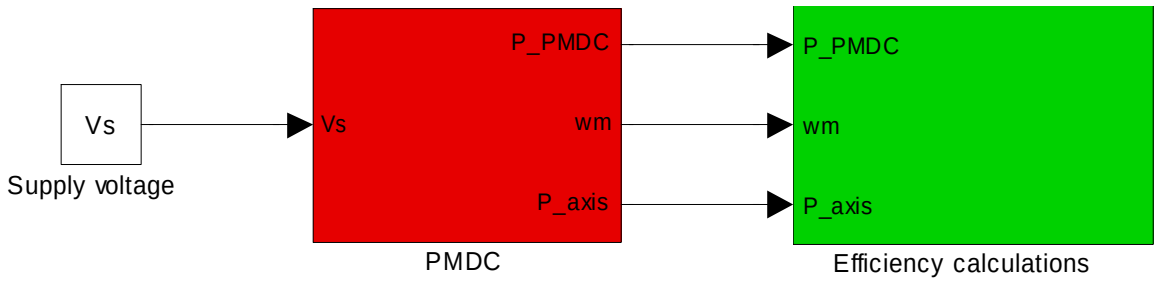

Figure 3.5: PMDC implementation

Figure 3.6 displays the PMDC block. The state space model inputs are the supply voltage, V_s and the load torque, T_L. The load torque is measured as a function of speed and is explained in section *4.2 Measurements of load.* Note that the load torque measurement includes the bearing friction, which is assumed to be the same for both motors. The outputs – the current i and the angular velocity ω are used to calculate PMDC power - P_PMDC and the output power on the rotor axis - P_axis is calculated according to *(3.3)*.

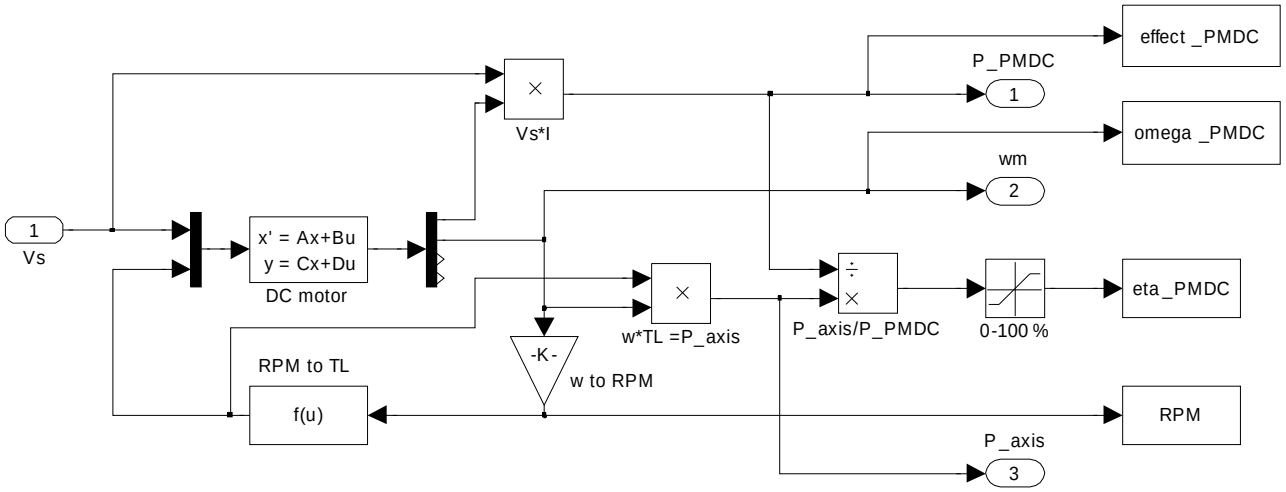

Figure 3.6: PMDC block

The output power is expressed as

$$P_{axis} = \omega_m T_L \tag{3.3}$$

and the efficiency is written as

$$\eta = \frac{P_{out}}{P_{in}} = \frac{P_{axis}}{P_{power\ electronic} + P_{PMDC}}. \tag{3.4}$$

The total efficiency for both driver and PMDC is calculated in the efficiency calculation block according to *(3.4)*. *Figure 3.7* displays the efficiency calculation block. Note that the power dissipated in the driver circuit is interpolated and implemented as a Matlab function and added to the PMDC power.

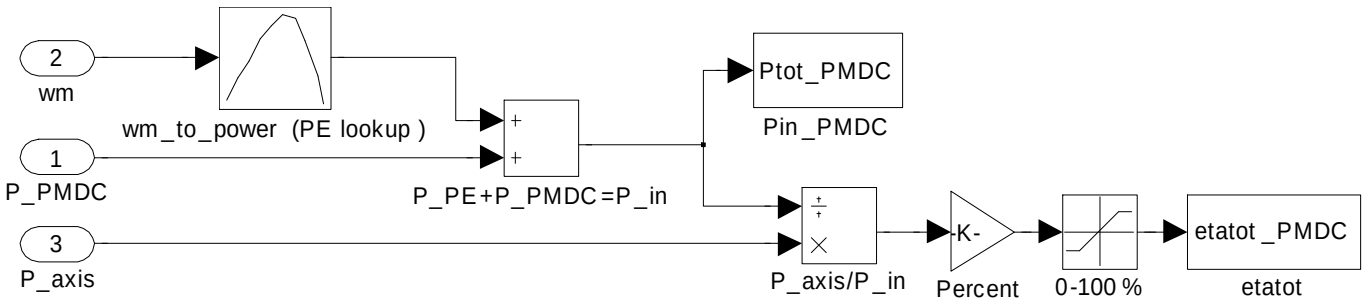

Figure 3.7: Efficiency calculation

3.2 Modeling BLDC motor

Implementations are made according to equations in section *2.4 BLDC*. By using *(2.7)* and *(2.8)* with the relation *(3.5)*, i_c can be neglected and the state space model can be implemented in Matlab/Simulink with four state-variables instead of five, which makes the simulation more efficient.

$$i_a + i_b + i_c = 0 \tag{3.5}$$

$$v_{ab} = R(i_a - i_b) + L\frac{d}{dt}(i_a - i_b) + e_a - e_b \tag{3.6}$$

$$v_{bc} = R(i_a + 2i_b) + L\frac{d}{dt}(i_a + 2i_b) + e_b - e_c \tag{3.7}$$

The state space model can be expressed as *(3.8)* and *(3.9)*. Note that the load torque T_L and BEMF e are dependent on previous outputs from the state space model.

$$\frac{d}{dt}\begin{pmatrix} i_a \\ i_b \\ \omega_m \\ \theta_m \end{pmatrix} = \begin{pmatrix} -\frac{R}{L} & 0 & 0 & 0 \\ 0 & -\frac{R}{L} & 0 & 0 \\ 0 & 0 & -\frac{k_f}{J} & 0 \\ 0 & 0 & 1 & 0 \end{pmatrix} \cdot \begin{pmatrix} i_a \\ i_b \\ \omega_m \\ \theta_m \end{pmatrix} + \begin{pmatrix} \frac{2}{3L} & \frac{1}{3L} & 0 \\ -\frac{1}{3L} & \frac{1}{3L} & 0 \\ 0 & 0 & \frac{1}{J} \\ 0 & 0 & 0 \end{pmatrix} \cdot \begin{pmatrix} v_{ab} - e_{ab} \\ v_{bc} - e_{bc} \\ T_e - T_L \end{pmatrix} \tag{3.8}$$

$$\begin{pmatrix} i_a \\ i_b \\ i_c \\ \omega_m \\ \theta_m \end{pmatrix} = \begin{pmatrix} 1 & 0 & 0 & 0 \\ 0 & 1 & 0 & 0 \\ -1 & -1 & 0 & 0 \\ 0 & 0 & 1 & 0 \\ 0 & 0 & 0 & 1 \end{pmatrix} \cdot \begin{pmatrix} i_a \\ i_b \\ \omega_m \\ \theta_m \end{pmatrix} \tag{3.9}$$

The Simulink implementation of the BLDC model, *figure 3.8*, consists of a commutation-, a BLDC- and an efficiency calculation block explained below. The input of the Simulink model is the supply voltage, V_s.

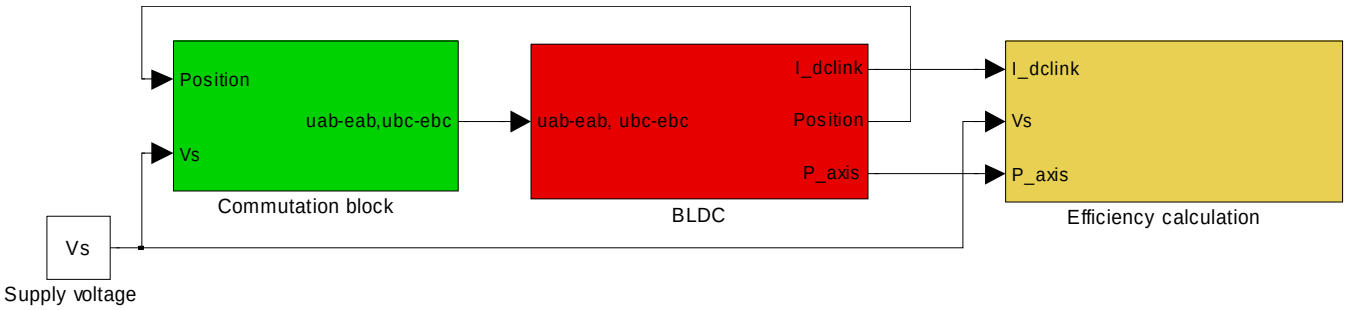

Figure 3.8: BLDC implementation

In order to commutate the BLDC motor properly, since its windings are switched separately, the task for the commutation block, see *figure 3.9*, is to resemble the six step commutation. By simulating the full bridge in *figure 2.6* with respect to rotor position and switch timings in *table 2.1*, an accepted algorithm has been implemented in the inverter block. The task of supplying the correct voltage over each winding at the right time, is dealt with in section *3.2.1 Inverter implementation*. The inputs are the rotor position in 60˚ interval to resemble the hall sensor, the supply voltage, V_s, the three phase currents zero crossing, I_{abcz}, and the BEMF, e_{abc}. The inputs are used to evaluate when each phase should be activated.

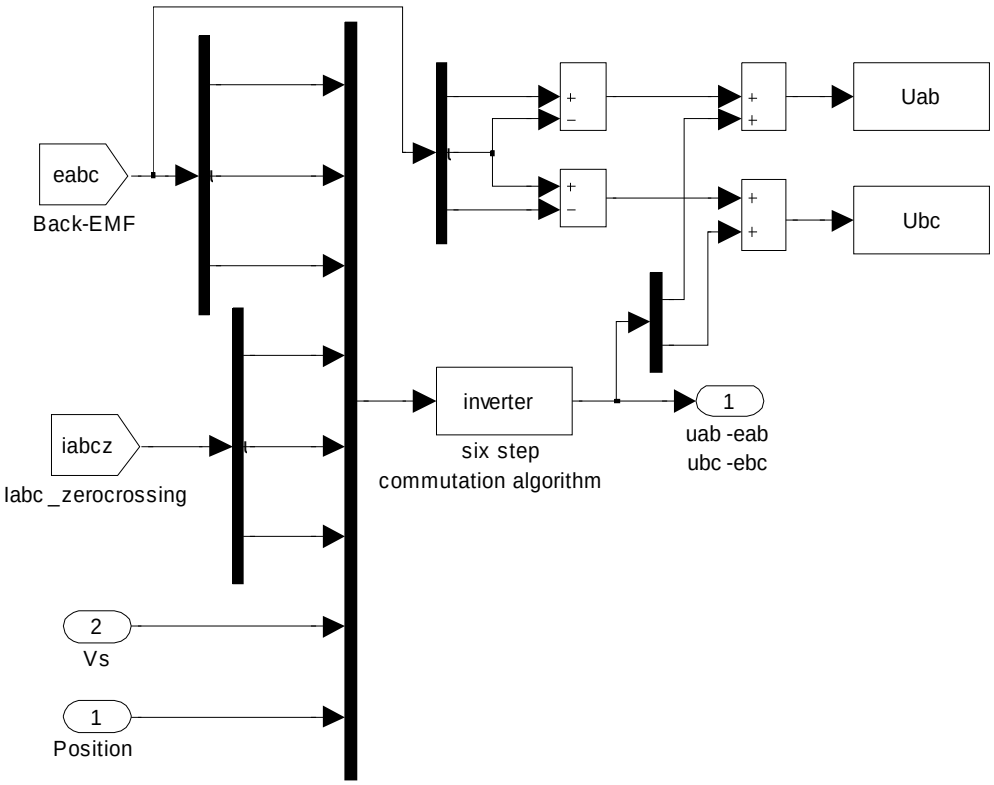

Figure 3.9: Commutation block

Figure 3.10 displays the BLDC main block. The inputs, U_{ab}-e_{ab} and U_{bc}-e_{bc} are fed forward to the state space model; *figure 3.11* and the input T_e-T_L are fed back from the Load block explained in *figure 3.12*. The BEMF and rotor position handling block is represented in *figure 3.13*. P_{axis} is calculated with *(3.3)*, the same equations as with the PMDC motor. The DC link current, I_{DClink} is expressed by summarizing the phase currents and dividing by two due to the fact that two phases are active at the same time which gives

$$I_{DClink} = \frac{\sum |I_a + I_b + I_c|}{2}. \tag{3.10}$$

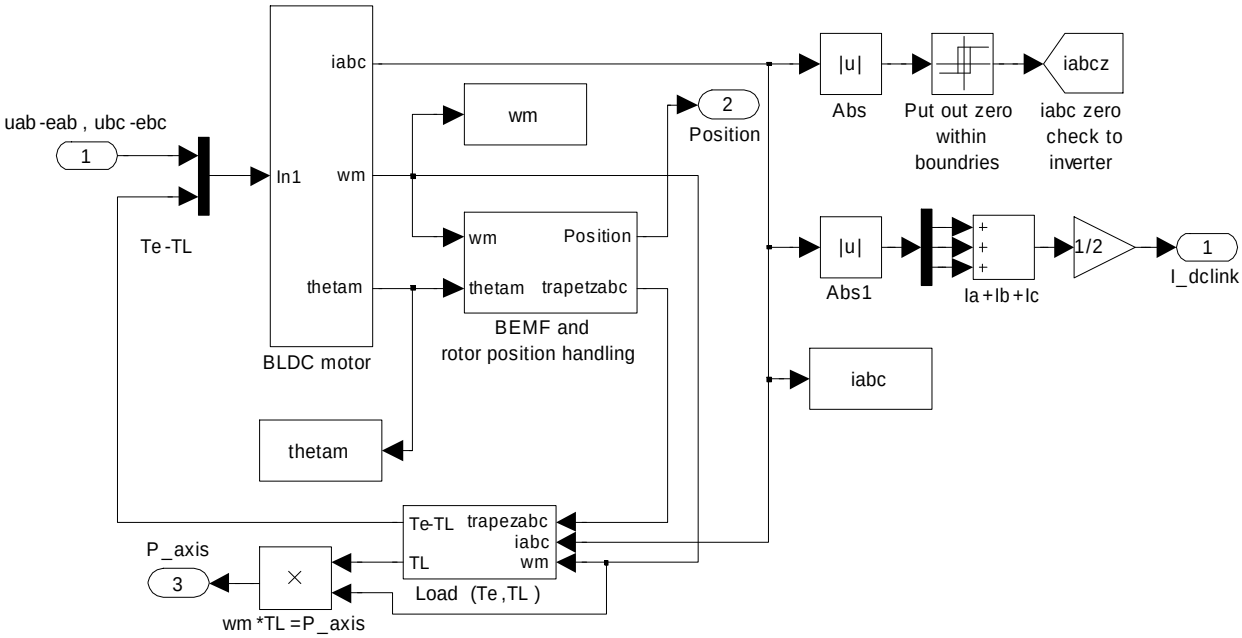

Figure 3.10: BLDC main block

The state space model is expressed by *(3.8)* and *(3.9)* and is implemented in the BLDC motor block, *figure 3.11*. Outputs are the three phase currents -i_{abc}, angular velocity -w_m and the angle of the rotor – $theta_m$.

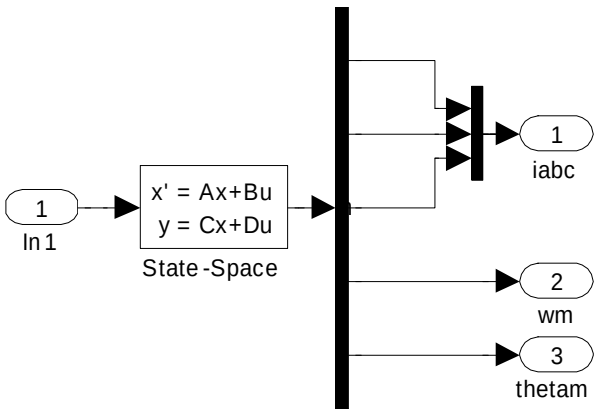

Figure 3.11: BLDC motor state space model

The load block, which feedback the T_e-T_L signal to the BLDC motor block, calculates the load torque according to the angular speed. The relation between load torque and angular speed is explained more in section *4.2 Measurements of load*. T_e is calculated according to *(2.14)*.

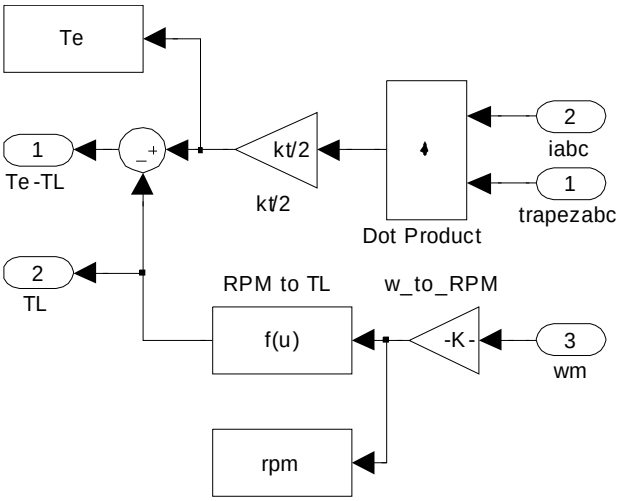

Figure 3.12: Calculation of T_e-T_L

The BEMF is simulated according to *(2.11)-(2.13)* to reach the trapezoidal shape and correct amplitude. The inputs are the constantly increasing mechanical angle, which is recalculated to electrical angle for one rotor revolution and the angular speed, w_m. The electrical rotor angle is fed forward through trapezoidal blocks that simulate the shape of the BEMF and gives the simulated hall sensor signals, see *figure 3.13.*

.

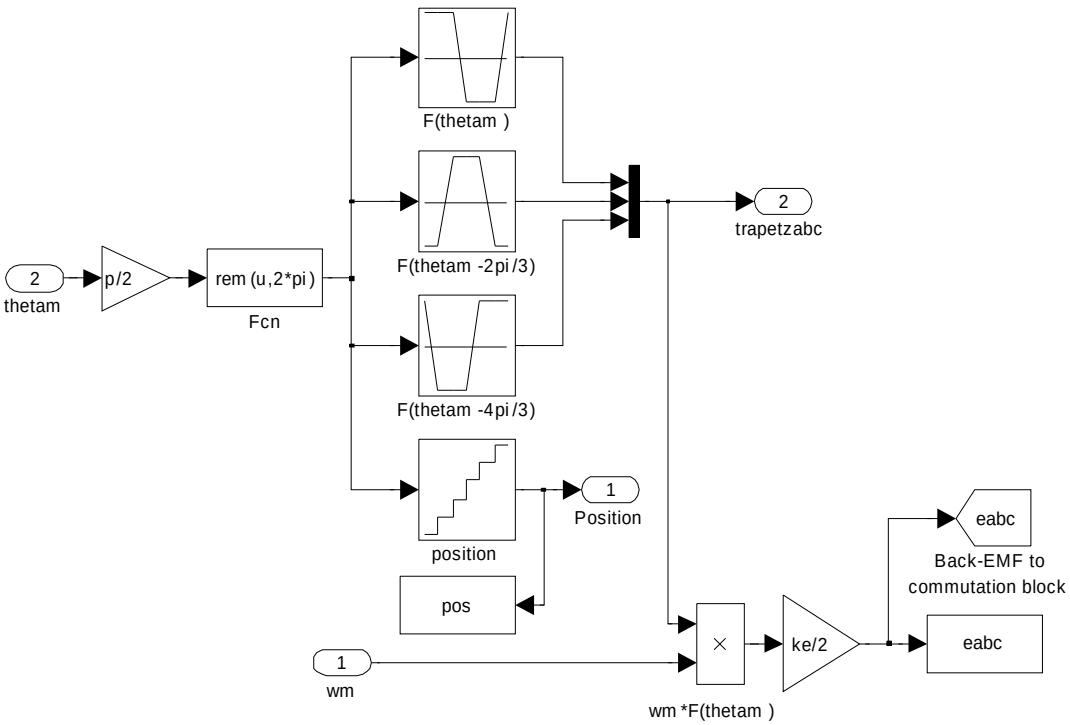

Figure 3.13: BEMF and rotor position handling

The efficiency is calculated as

$$\eta = \frac{P_{out}}{P_{in}} = \frac{P_{axis}}{P_{BLDC}} = \frac{P_{axis}}{V_s I_{dclink}}. \tag{3.11}$$

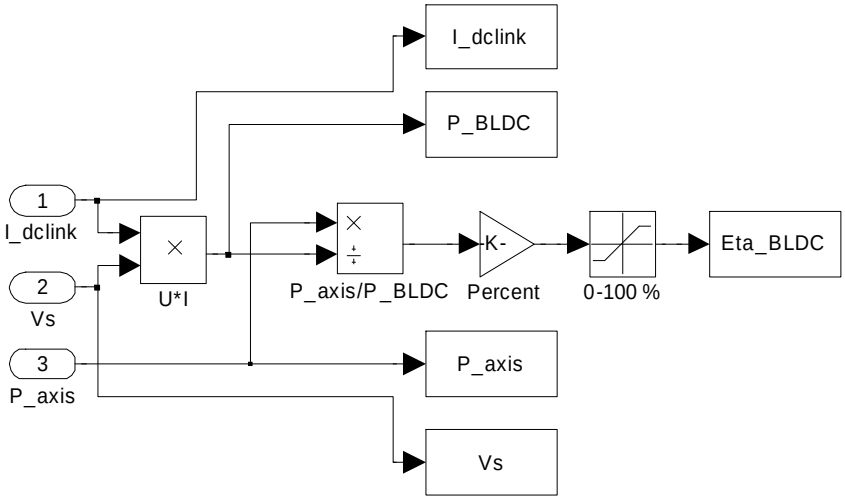

Figure 3.14: Efficiency calculation

3.2.1 Inverter implementation

The equivalent scheme of the motor and its driver is the circuit containing the stator winding impedance Z, the supply voltage V_s and each phase BEMF e, see *figure 3.15*. Depending on which direction the currents flow, a switch $SW_{supplyvoltage}$ will change the polarity of V_s and depending on when currents decline through the freewheel diodes, a switch $SW_{freewheel\ diode}$ models when the freewheeling diode currents are zero or not. The latter is explained in *figure 3.16*.

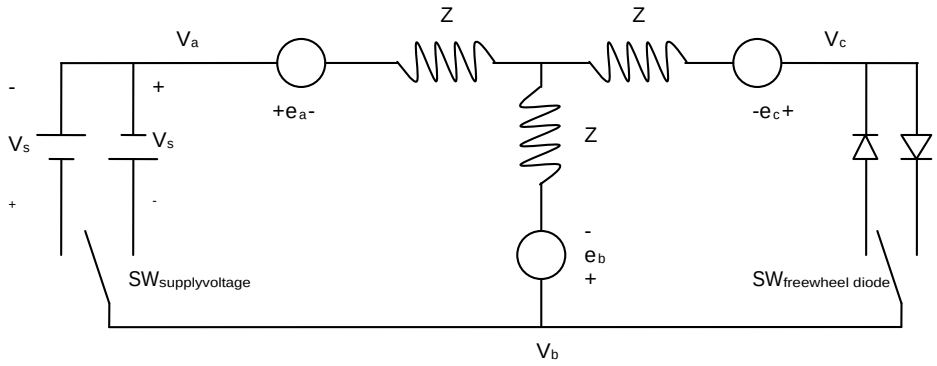

Figure 3.15: Equivalent circuit six step commutation

To develop a good approximation when to energize each stator winding, it is necessary to analyze how the currents in the machine flow during the six step commutation. *Figure 3.16* is based on section *2.5.2 Sensor driven BLDC* and explains when the freewheeling diode currents are zero or not. This information is taken into account when drawing *table 3.1* below.

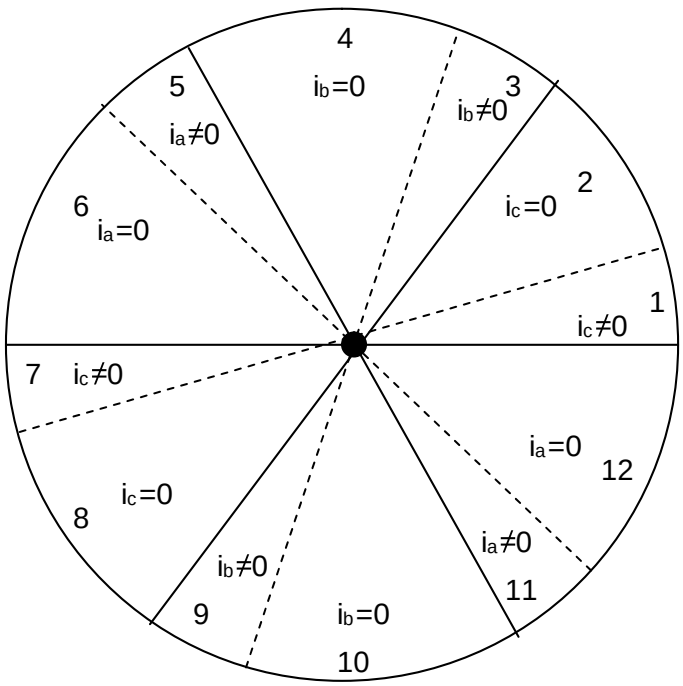

Figure 3.16: One electrical revolution in six step commutation

Since one electrical revolution is divided into six steps, *table 2.1* only gives the information of phase voltage during commutation time, there is also a need to extend this table with information of when currents freewheels through the diodes, see section *2.5 BLDC drives*. The extension gives another six sequences to consider when drawing *figure 3.16* and sums up to twelve commutation sequences depending on the freewheeling currents.

By analyzing the equivalent circuit in *figure 3.15* with Kirchhoff's current law and Kirchhoff's voltage law together with *figure 3.16*, equations of the six step commutation can be derived. The results of the analysis above is represented in *table 3.1: Inverter output voltages for one electrical revolution in six step commutation* below where V_{ab} and V_{bc} are expressed in terms of the BEMF and supply voltage. The commutation sequence is now extended with the freewheeling currents through the diode. The results in *table 3.1* are the basic algorithm that is implemented in the inverter block in the Simulink BLDC model, see *figure 3.9*.

Table 3.1: Inverter output voltages for one electrical revolution in six step commutation

Commutation sequence	Electrical angle	V_{ab}	V_{bc}
1	0-60˚	V_s	0
2	0-60˚	V_s	$\frac{1}{2}(-V_s+e_a+e_b)-e_c$
3	60-120˚	0	V_s
4	60-120˚	$\frac{1}{2}(V_s+e_a+e_c)-e_b$	$\frac{1}{2}(V_s-e_a-e_c)+e_b$
5	120-180˚	$-V_s$	V_s
6	120-180˚	$-\frac{1}{2}(V_s+e_b+e_c)+e_a$	V_s
7	180-240˚	$-V_s$	0
8	180-240˚	$-V_s$	$\frac{1}{2}(V_s+e_a+e_b)-e_c$
9	240-300˚	0	$-V_s$
10	240-300˚	$\frac{1}{2}(-V_s+e_a+e_c)-e_b$	$-\frac{1}{2}(V_s+e_a+e_c)+e_b$
11	300-360˚	V_s	$-V_s$
12	300-360˚	$\frac{1}{2}(V_s-e_b-e_c)+e_a$	$-V_s$

4. Results

4.1 Measurement set up

The two motors operate the same fan at the same position as can be seen in *figure 3.1*. The fan is to operate with nothing blocking the air flow throughout all of the measurements to get comparable results and the same measuring procedure is applied to the two motors.

Both motors produce currents and voltages that can not be regarded as fix values of DC quantities. When measuring currents and voltage from the motors an oscilloscope is used to calculate mean value over a large number of periods to get usable results. The measurement error analysis can be found in *Appendix B.*

Table 4.1 shows the devices used during measurement.

Table 4.1: Data Acquisitioning tools

Device	Model	Serial Number
Power supply	Delta Elektronika SM 35-45	993
Oscilloscope	LeCroy Wavesurfer 434	994
Multimeter	Fluke CHY 14	575
Current probe	Fluke 80i-110s	-
Current probe	LeCroy AP015	-
Tachometer	Lutron DT-1236L	-
Scale	Mettler PM30-K	-

4.2 Measurements of load

To be able to measure efficiency of the two motors the load needs to be measured. Load torque is multiplied by speed and gives the load power. The measurement set up can be seen in *figure 4.1* below.

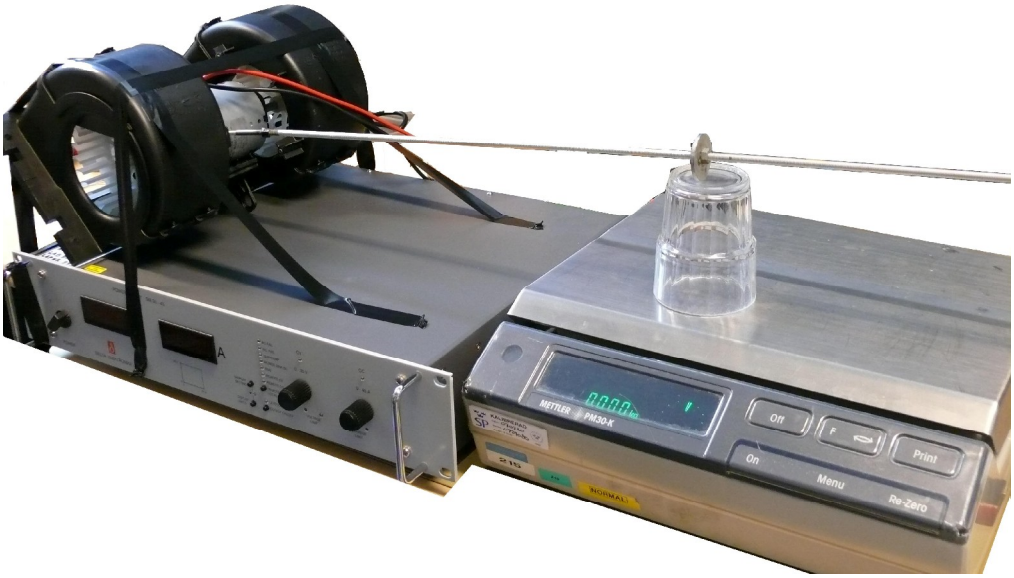

Figure 4.1: Torque measurement

The torque acting on the fan from the airflow is compensated by the reverse torque acting on the motor. Usually the motor is fixed but in these measurements it can easily roll in its fittings carrying the reverse torque through the axis that is fitted to the DC motors housing. To furthermore reduce friction the fittings and the motor is lubricated. The force F of the axis length L meters away from the turning center is measured by a high end scale. To gain in scale accuracy means that the axle should be as short as possible to increase the equivalent mass weight. To discard the weight offset, m_{0rpm}, at zero rpm at the scale it is subtracted from the measured weight, m_{xrpm} and the torque, T is calculated as

$$\begin{cases} F = mg \\ T = FL \end{cases} \Rightarrow T = (m_{Xrpm} - m_{0rpm})gL\,. \qquad (4.1)$$

With a lever axis of 0.5 meter, the torque is given by multiplying the equivalent mass multiplied by *g* divided by two, where *g* denotes the gravity constant. The measurement error analysis can be found in *Appendix B.* The result from different speeds can be seen in *figure 4.2*.

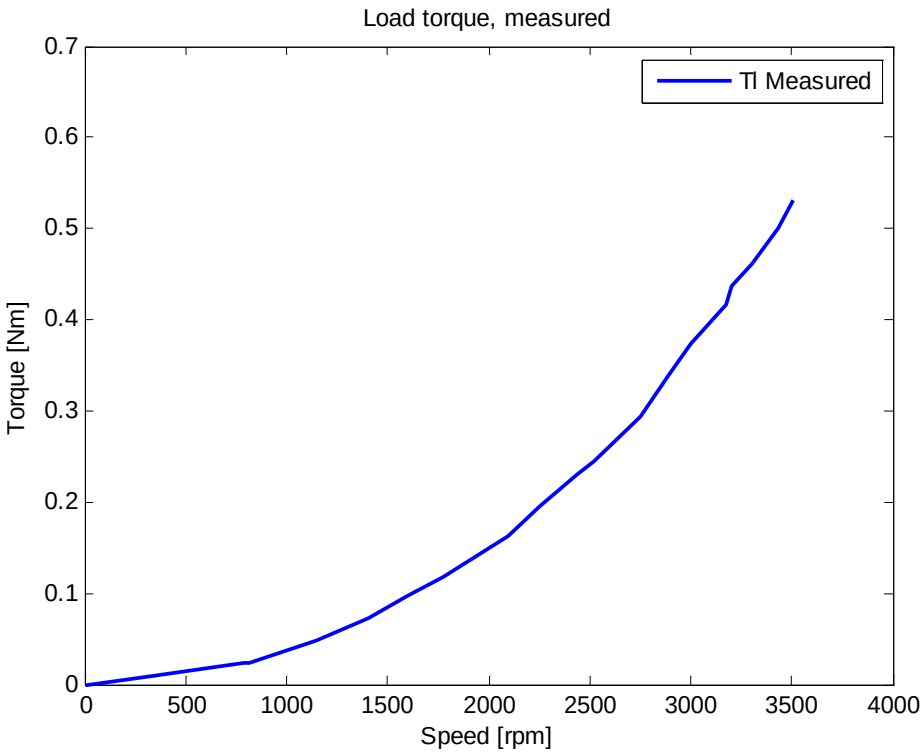

Figure 4.2: Measured load of fan application

As can be noted from *figure 4.2*, the load behavior increases exponentially, as expected with a fan application. These values are then interpolated to an equivalent function and used in the simulation. Note that this load torque includes the bearing friction which may be different from machine to machine.

4.3 Results of PMDC motor

The parameters of the PMDC (R, L) were measured and the flux constant - K_e derived from *(2.2)*. For measurement error analysis, see *Appendix B*.

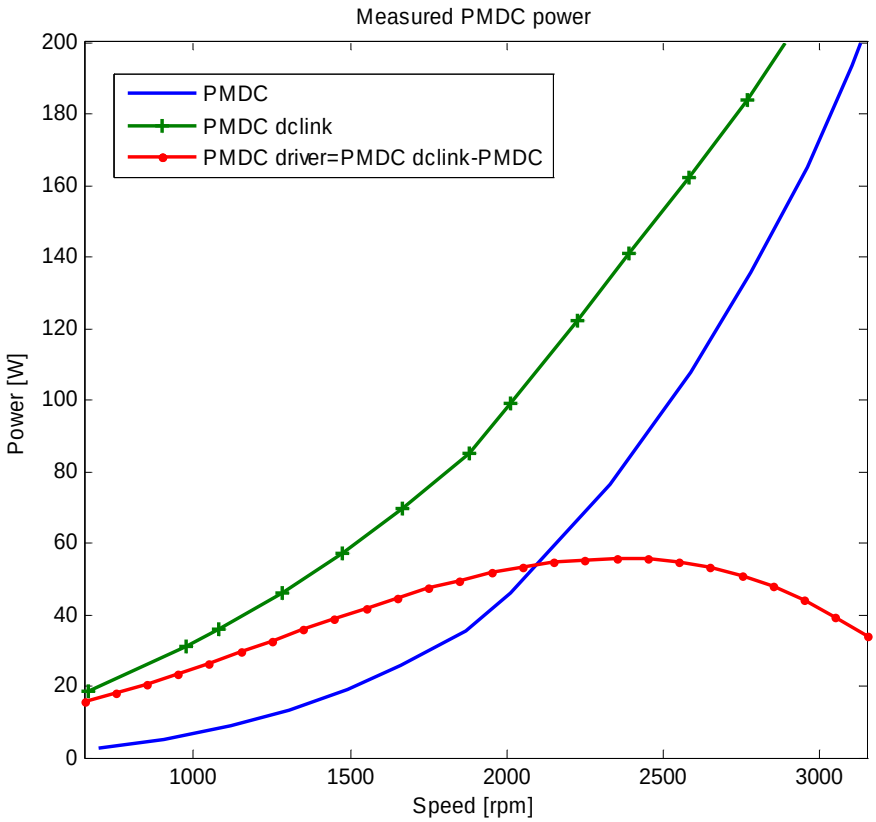

Figure 4.3: Measured power relations of PMDC fan application.

In *figure 4.3* the room for improvement is considerable, especially for the PMDC driver at low speeds which ironically is where this compartment fan normally operates in steady state after cooling/heating the truck compartment. By improving the power electronics efficiency, a great increase in overall efficiency can be achieved.

Figure 4.4 displays the simulated PMDC fan application from section *3.1 Modeling PMDC*. The simulated results are very close to the measured, compare with *figure 4.3*. The deviations are due to iron losses in the stator and changing flux and brush resistance over changing temperature. By implementing more nonlinear elements and dependencies in the model, a better approximation can be reached. Note that the power dissipated in the PMDC driver is measured and simulated by a look up table.

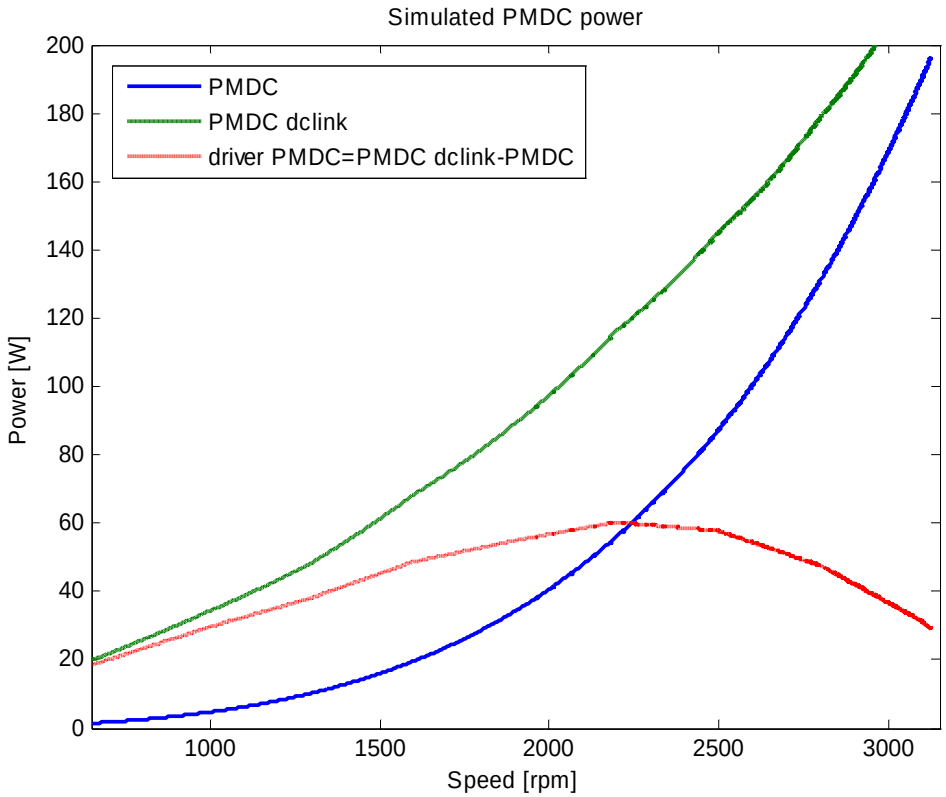

Figure 4.4: Power relations of simulated PMDC fan application.

4.4 Results of BLDC motor

4.4.1 Two watt meter method

Measuring power consumption in a three phase motor is more difficult than in the PMDC case. First, because of the switched waveforms a high sample rate is required which generate lots of data. A high sampling rate together with *(4.1)* below yields the three phase mean power in one period if the three phase currents are equal, implying that all three have the same inductance and resistance in the windings.

$$P_{3\Phi} = \frac{3}{nT}\int_0^{nT} u_\Phi i_\Phi dt \tag{4.1}$$

It is often difficult to measure voltage in a three phase Y winded BLDC motor over one phase due to the absence of the point where the windings meet. An alternative way is to use a method called the two watt meter method [11] as can be seen in *figure 4.5*.

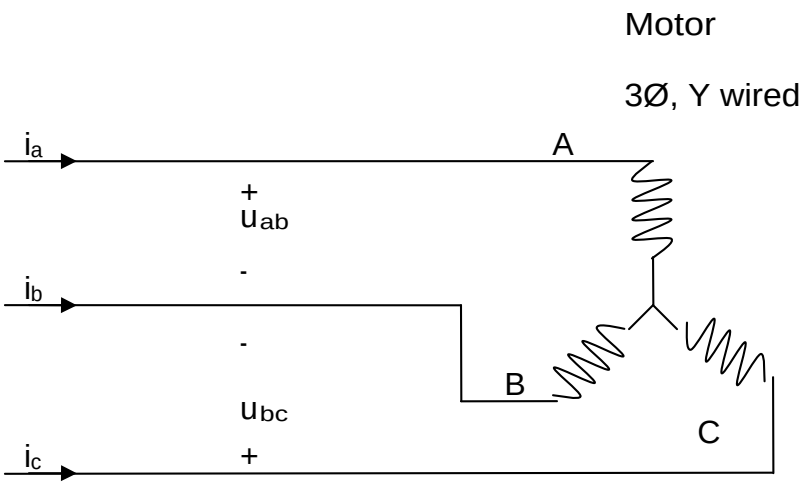

Figure 4.5: two watt meter method

The zero winding is not connected and carry no current. Kirchhoff's current law yields

$$i_a + i_b + i_c = 0 \Rightarrow i_b = -(i_a + i_c) \tag{4.2}$$

Starting from (*4.1)* and combining with (*4.2)*

$$P_{3\Phi} = \frac{1}{nT}\int_0^{nT}(u_a i_a + u_b i_b + u_c i_c)dt \Rightarrow (4.2) \Rightarrow \frac{1}{nT}\int_0^{nT}(u_a i_a - u_b(i_a + i_c) + u_c i_c)dt = \frac{1}{nT}\int_0^{nT}(u_a - u_b)i_a + (u_c - u_b)i_c)dt = \frac{1}{nT}\int_0^{nT}(u_{ab} i_a + u_{cb} i_c)dt. \tag{4.3}$$

The simulation results are simulated from a modified BLDC model, with a sinusoidal shape of the BEMF instead of a trapezoidal shape in the case when having a BLDC motor. This modification is made since further experiments made on the Motion King motor showed that its actual BEMF had a sinusoidal shape, hence the motor is a PMSM but driven by a six step commutation BLDC drive.

Figure 4.5 displays the currents and voltage over phase A-B.

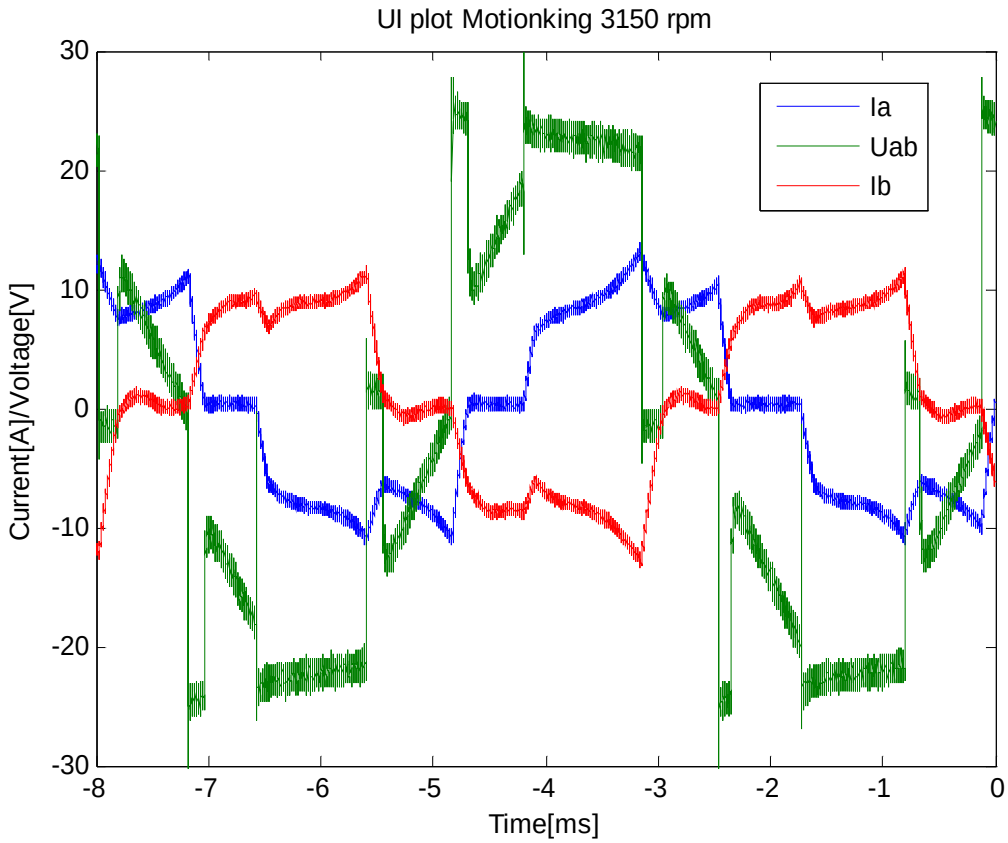

Figure 4.5: Measured voltage and currents at 3150rpm

Appendix C contains the three phase currents and voltages.

Figure 4.6 shows the simulated equality to the measured values in *figure 4.5*. As can be noticed, the shape looks ideal and the switching algorithm for energizing the stator winding A-B is working properly. Levels of both currents and voltages are fundamentally correct but can be further improved by adding the non linearity of the winding resistance and inductance dependencies of speed. This alters the copper losses and changes the magnetic flux.

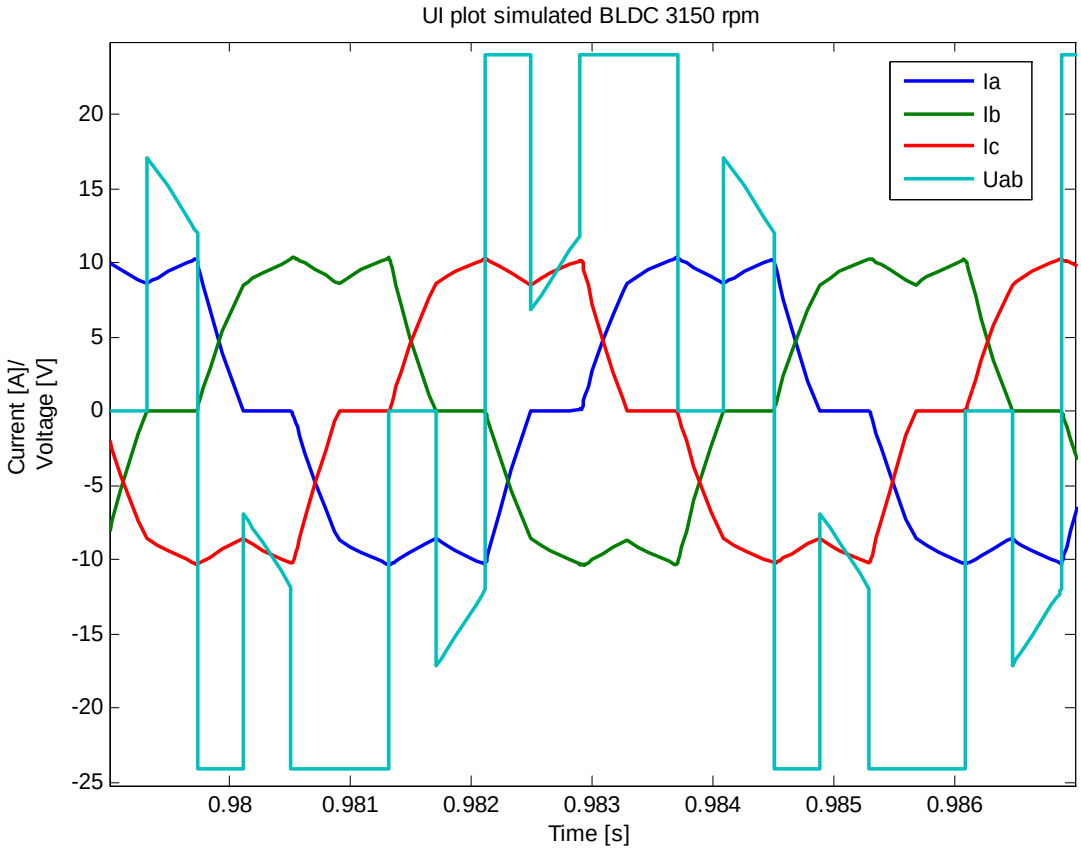

Figure 4.6: Simulated voltage and currents at 3150rpm

Figure 4.7 displays the withdrawn BLDC motor power and the BLDC system power. Note that there is almost no difference between them implying that the driver operates with a high efficiency and that the difference between the BLDC motor and the BLDC DC link lies within the interval of measurement errors.

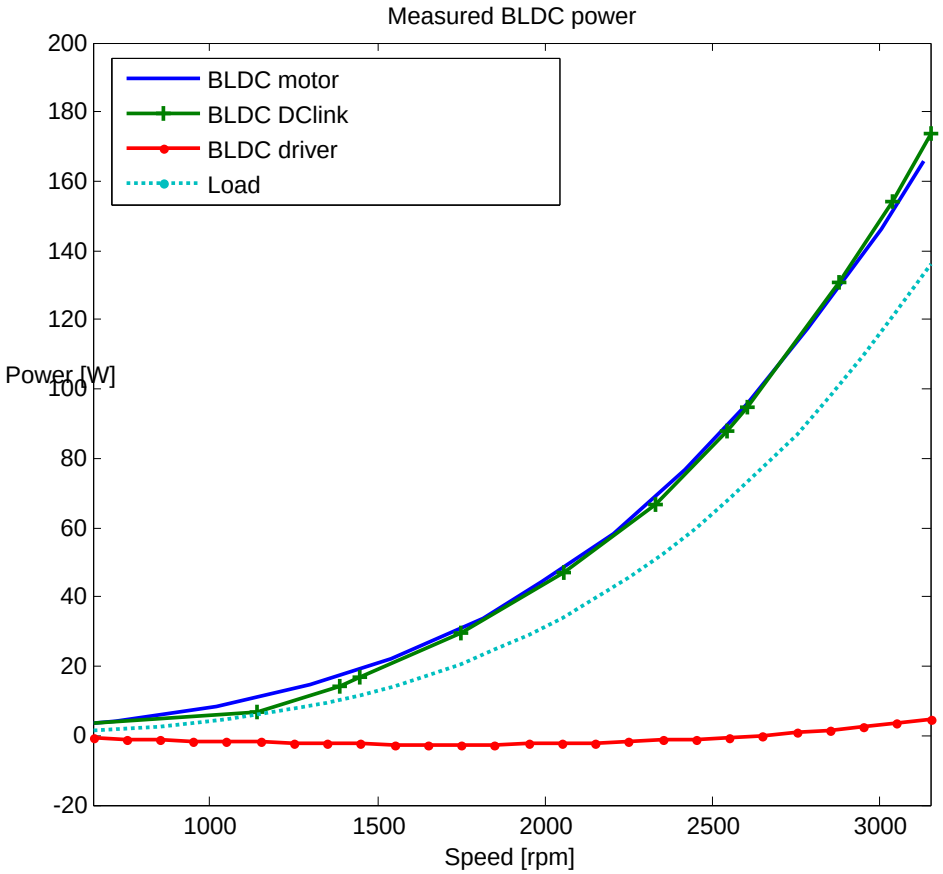

Figure 4.7: Measured power relations BLDC fan application.

Figure 4.8 displays the power withdrawn from the simulated motor when the applied load is a simulated fan. At high speed the motor needs more power to rotate the loaded rotor axis which is correct and at low speed, the load curve lies above the BLDC curve, which indicates that the motor needs less power then the load curve demands. This result is wrong since the output power always is less then input power, else an efficiency of more than 100% are achieved. These problems are due to simulation difficulties which lead to wrong calculated efficiency, see *figure 4.15*. One explanation of this behavior is that the model is very simplified and needs to be extended with more nonlinearity effects.

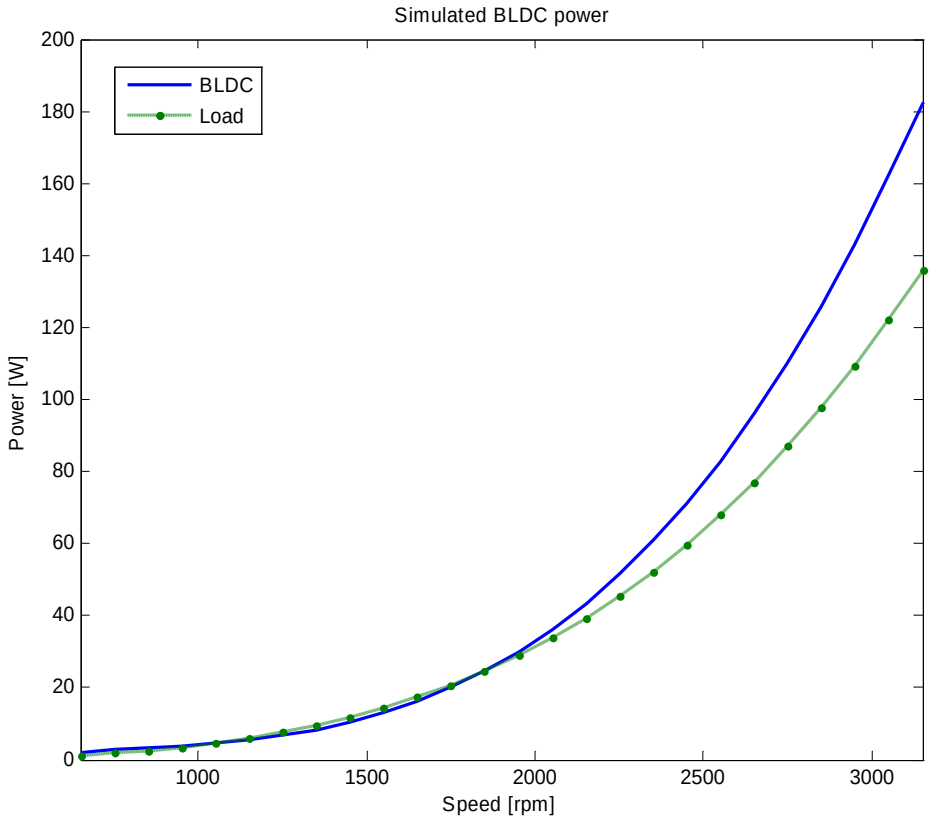

Figure 4.8: Simulated power relations BLDC fan application.

4.4.2 Sensor less PMSM driver

The delivered BLDC motor's BEMF were measured and it was assumed [31] that it would be possible to run with sinusoidal voltages instead of the proposed six step commutation above. For the automotive industry there is no economical room for the absolute encoder for position sensing which forces the PMSM driver to be operated sensor less. This is possible with the development board IRMCS 2033, see *figure 4.10* from International Rectifier, which uses FOC control, seen in *figure 4.9*. The FOC control is applied after a start up sequence similar to the BLDC sensor less startup in section *2.5.3.1 Start up strategy*, where the rotor is aligned and then a forced drive is used before the flux estimator can operate. All parameters need to be known within a ten percent error interval and are stored to the microprocessor via serial RS232 communication. These parameters are roughly estimated for the Motion King motor and may not be optimized for efficiency.

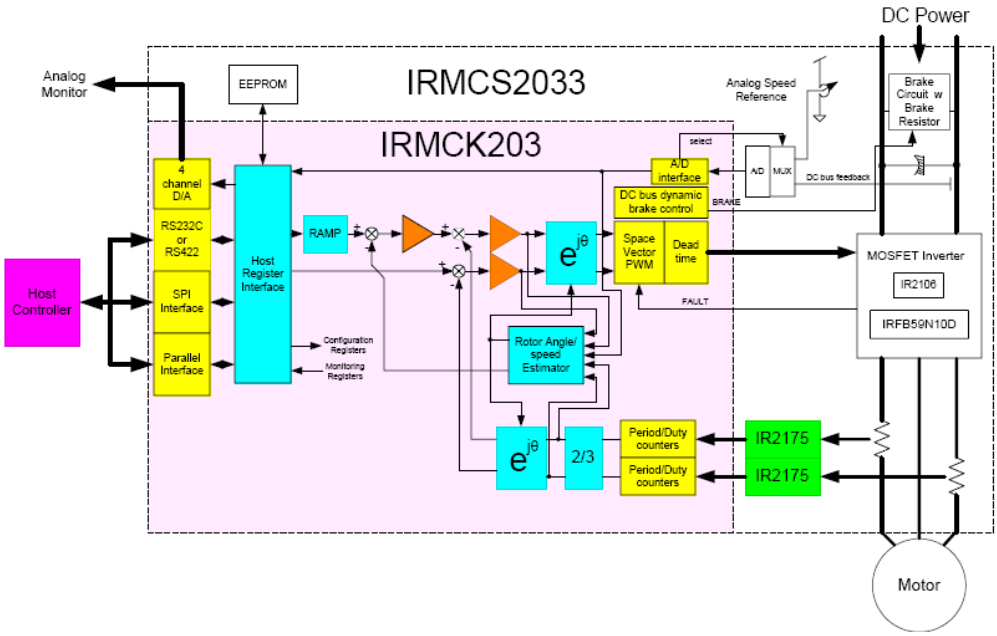

Figure 4.9 – schematic view of sensor less PMSM drive, courtesy of IR

Figure 4.10 –physical view of sensor less PMSM driver, courtesy of IR

4.5 Comparisons

The DC link currents drawn from the 24 V power supply can be seen in *figure 4.11*. The BLDC current rises every time a phase is energized. For the BLDC, it can be noted that

3150 *mech rpm* = 52.5 *mech rpm / s* $\Rightarrow$ 1 *mech rev* $\approx$ 19 *ms*

19 ms/(8 poles*3 phases) = 0.79 *ms.*

This implies 0.79 ms between the excitation of each phase. A zoomed view of the BLDC spikes gives, as calculated, a time interval in the approximate range of 0.8 ms.

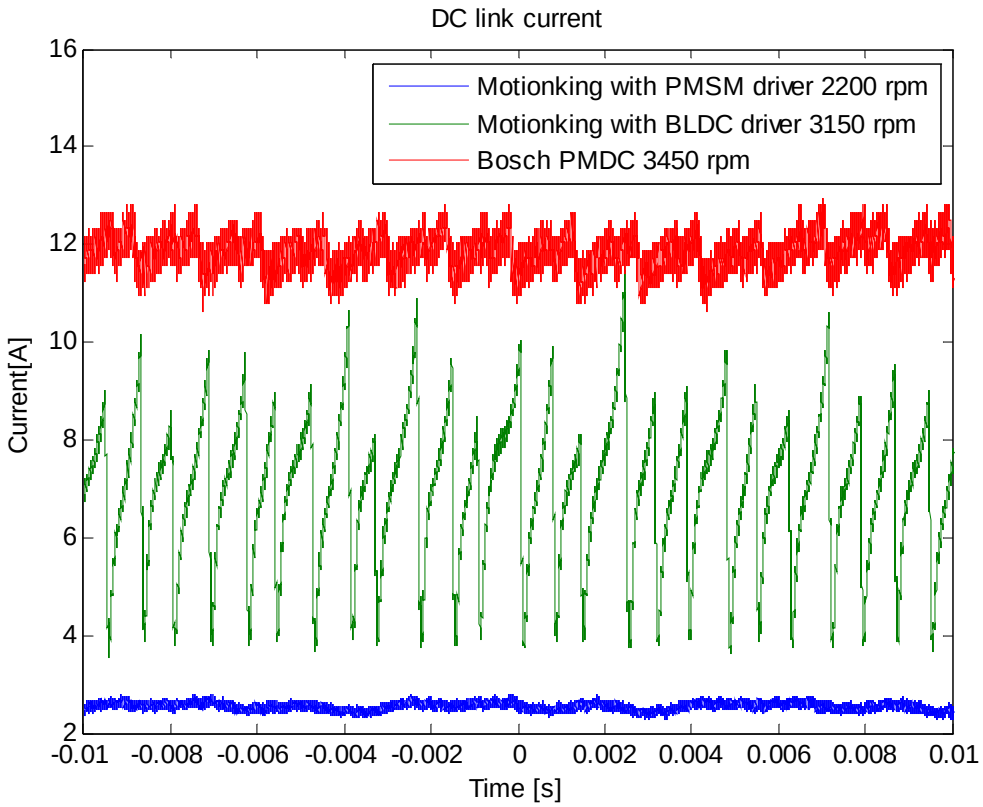

Figure 4.11 – Dc link currents PMDC/ BLDC/PMSM

These current spikes directly imply that there can be torque ripple which is a well known problem of the BLDC motor which produces harmonics that could yield an EMC problem. These could be minimized by using a decoupling capacitor. For both the PMSM driver and the PMDC driver the current ripple is less prominent. Note that the three DC link currents are presented at different speeds.

The motor power, excluding the driver, for the BLDC- and PMDC motor, can be seen in *figure 4.12*. At low speeds the motor powers are comparable, but the presence of the resistive voltage drop from the brushes in the PMDC can be seen at high speeds, due to the increased deviations between the two motors. Calculations show that this improvement is 14 % at 3150 rpm.

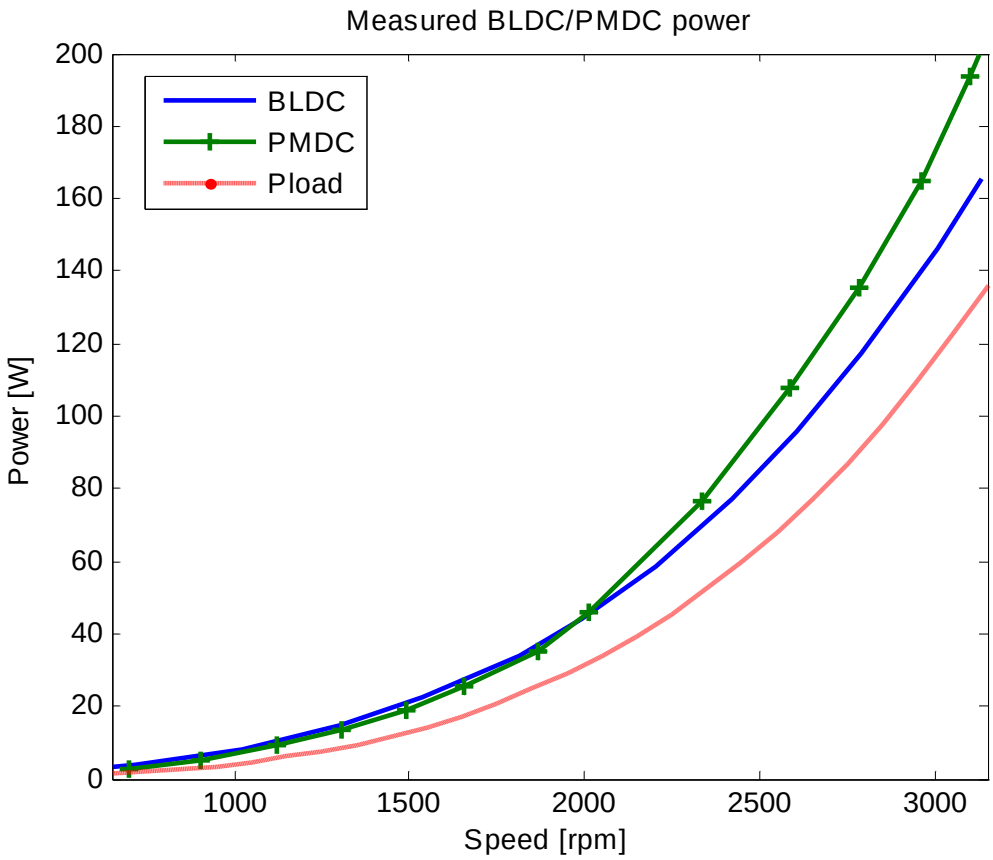

Figure 4.12 – Measured motor power BLDC/ PMDC

The major differences when comparing the total power consumption can be seen when measuring the DC linkage in *figure 4.13*. The efficiency of the driver influences on the total power withdrawn from the power source. The savings curve has its peak around 2750 rpm's and has a mean value of 50 watts over the whole speed interval.

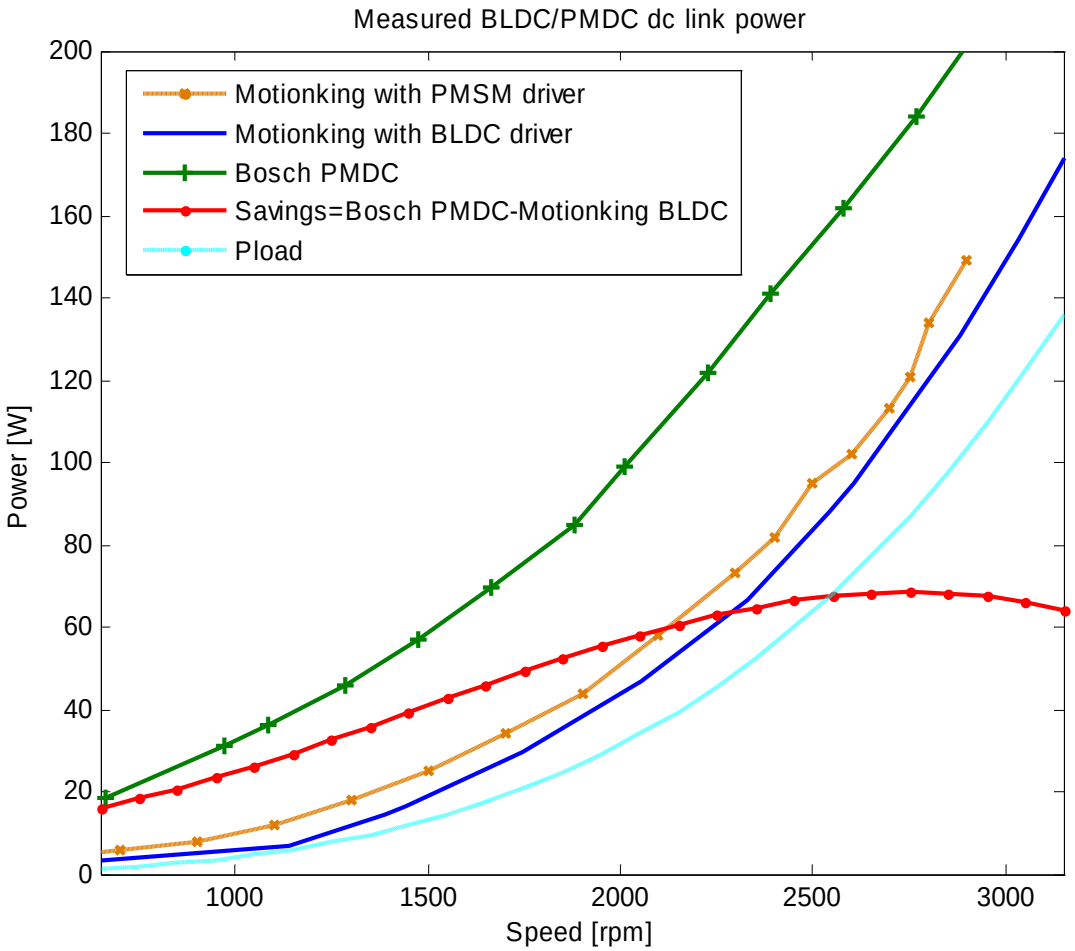

Figure 4.13 – Measured power drawn from the DC link

The overall efficiency of the BLDC system is superior to the PMDC and its driver. Comparing the efficiency of the two motor types gives higher efficiency for the BLDC motor. In *figure 4.14*, the BLDC curve is lower than the BLDC & Driver curve which is due to measurement errors, i.e. differences when measuring three phase effect and DC link power. The comparison of the two systems mounted in each fan application indicates an increase of efficiency, especially below 2000 rpm where the compartment fan normally operates in steady state after a cooling or heating sequence depending on ambient temperature [12].

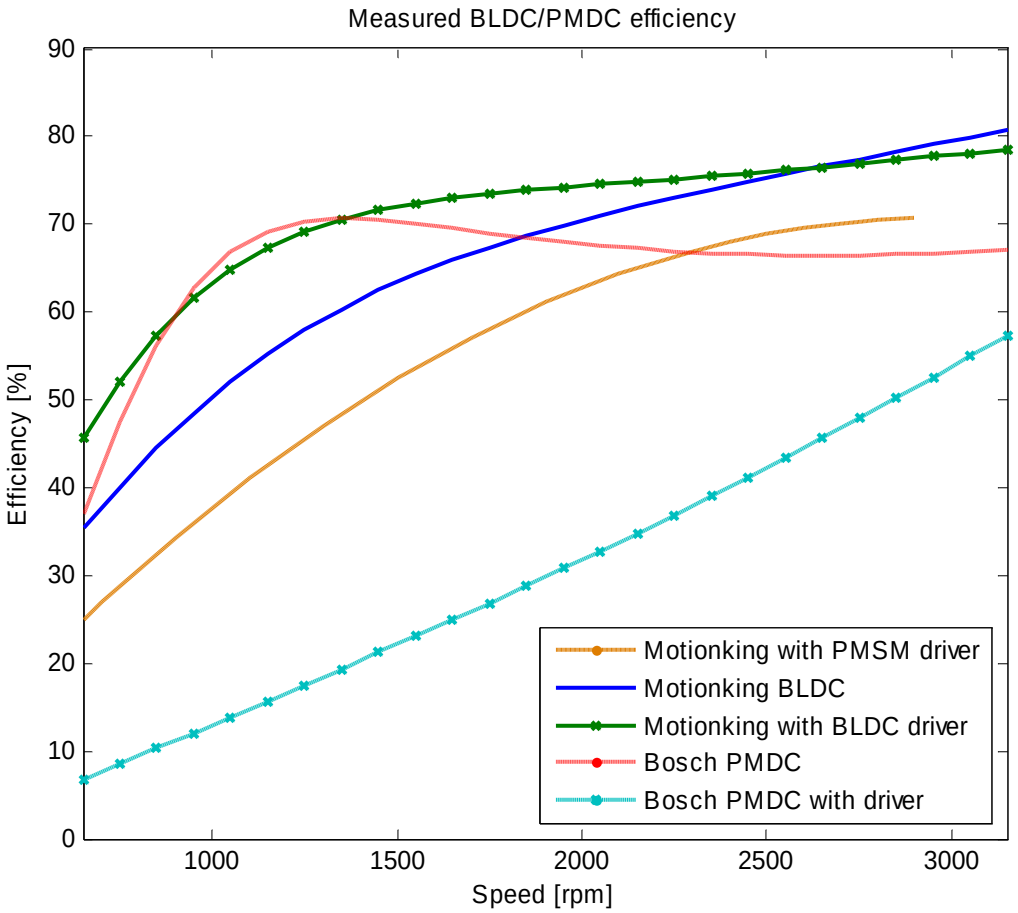

Figure 4.14: Measured efficiency PMDC/BLDC fan application

At 3150 rpm the efficiency increase for the new BLDC system is 21 % and the increase when the BLDC system is compared to a PMDC operated without the driver, i.e. with a circuit breaker, is 12 %. Note that the measured PMSM driver parameters may not be optimized which could result in a lower efficiency due to non ideal sinusoidal motor currents.

Simulating efficiency of both the PMDC and the BLDC is a study for improvement. The PMDC & driver efficiency is close to the measured results in *figure 4.15*. Both the shapes and the values are near measured. The simulated BLDC efficiency has both shape and value deviations compared to the measured results due to non linear effects that has not been implemented in the model. The values above 100% of the BLDC curve are not realistic, *see page 46*.

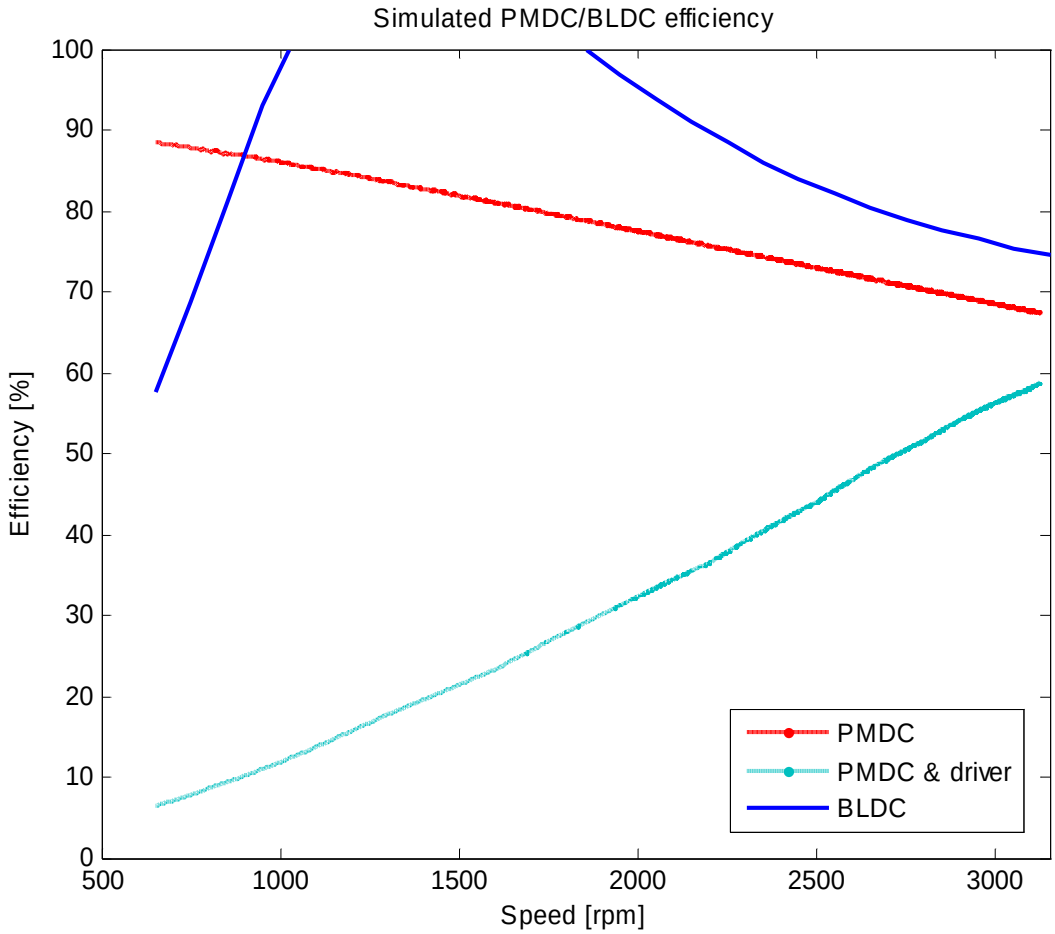

Figure 4.15: Simulated efficiency of PMDC/BLDC fan application

4.6 Case studies

The electrical savings for the rebuilt BEHR fan is averaged 50 watts over the entire speed interval. For a long haul truck operated at 3000 h annually together with assumptions [13], the following is obtained.

$$\left.\begin{aligned}
&\eta_{generator} = 60\%, mean \\
&\eta_{ICE,diesel} = 35\%, mean \\
&E_{diesel} = 44MJ/Kg \\
&\rho_{diesel} = 0.86kg/l \\
&P_{electric}^{saved} = 50W \\
&t_{usage}^{annual} = 3000h
\end{aligned}\right\} \Rightarrow E_{savings} = \frac{P_{electric}^{saved}}{\eta_{generator} \cdot \eta_{ICE,diesel}} \cdot t_{usage}^{annual} \cdot 3600 \approx 25.7 \cdot 10^8\, J$$

$$Diesel_{savings} = \frac{E_{savings}}{E_{diesel} \cdot \rho_{diesel}} \approx 70\ liters \Leftrightarrow 190\ kg\ CO_2 \quad (4.4)$$

A Volvo articulated city bus of today has two separate air ventilating units, one for the driver to ensure driving safety and one for the passenger compartment. The fans for the passengers consists of ten 280 W brushed DC motors and for the driver fan it is assumed to be equal to the truck fan discussed above. With air-conditioning, the top cooling capacity of the passenger system is several tens of kW.

Assuming that the passenger fans are constantly operated at maximum speed, only operated with a circuit breaker, together with the measured saving of 12 % for the transition between PMDC- to BLDC motors the following is found.

$$\left.\begin{aligned}
&\eta_{generator} = 60\%, mean \\
&\eta_{ICE,diesel} = 35\%, mean \\
&E_{diesel} = 44MJ/Kg \\
&\rho_{diesel} = 0.86kg/l \\
&P_{driver\ fan}^{saved} = 50W \\
&P_{passanger\ fan}^{saved} = 10 \cdot 280W \cdot 12\% \\
&t_{usage}^{annual} = 4000h
\end{aligned}\right\} \Rightarrow E_{savings} = \frac{P_{electric}^{saved}}{\eta_{generator} \cdot \eta_{ICE,diesel}} \cdot t_{usage}^{annual} \cdot 3600 \approx 2.65 \cdot 10^{10}\, J$$

$$Diesel_{savings} = \frac{E_{savings}}{E_{diesel} \cdot \rho_{diesel}} \approx 700\ liters \Leftrightarrow 1900\ kg\ CO_2 \quad (4.5)$$

With an assumed diesel value of 10 SEK / liter and with a calculated additional cost of 300 SEK per BLDC motor the pay off time is about half a year. This implies that there is an economical potential to use the more expensive BLDC motor.

5 Conclusions

For the cost sensitive automotive industry, the brushless PM motors are most likely to operate sensor less to furthermore reduce cost for cabling and sensors. The hall sensors are also a source of malfunction and a small mounting offset in the sensors gives a suboptimal commutation.

The sensor less operation techniques of today is most appropriate for fan and pump applications with low starting torque as there might be a problem during start up. A sensor less controller using the measurement of the zero crossing with comparators for the zero crossing signals is usable but the software must not only be complemented with the 30 degrees delay after a zero crossing and a startup technique but also a way of filtering the comparator signal. Furthermore, the software should be programmed with a sequence that generates optimal commutation to obtain a gain in efficiency.

The rebuilt BLDC application gives an efficiency of 80 % at full speed. A sensor less six step commutated BLDC with optimal commutation fixing code in the range of the Motion King motor handled in this report may end up at 85 % efficiency. PM motors operating at higher speeds at the same power range gives lower torque due to lower currents which reduce copper losses and makes the motor gain in efficiency.

The PMDC motor suffers from lower efficiency than the brushless PM motors but can as a system gain in efficiency by using a PWM driver instead of the linear driver used today. Even though, a PMDC motor with a PWM driver will not reach the efficiency of a BLDC system.

The six step commutation enables 15 % more power density compared to a sinusoidally fed PMSM but the PMSM gains from lower torque ripples, lower acoustic noise and lower EMC problems. To operate a PMSM in sensor less mode requires more computer power than the sensor less six step commutation, but as the cost for computer power decreases, it is also possible to enable some synergy effects as CAN communication for feedback of motor speed and error messages to get a more robust system.

Simulation of efficiency with the aim to resemble measurements for the entire speed interval is difficult for the PMDC and BLDC motors. Both the PMDC and BLDC model used in this report needs to be extended to include nonlinearities for the resistance and inductance, i.e. a speed dependency on the copper losses and the magnetic flux due to mutual inductance between windings. To understand the behavior of the machines the models are usable. There is also a problem to get correct values of motor parameters from the manufacturers as each motor varies.

The lifetime of brushless PM motors seems only to be limited by the axle bearings as the electronic is regarded to have a longer lifetime, in the range of 3 to 5 times longer compared to the life time of a brushed DC motor.

6 Discussion

For the rebuilt actuator to save fuel there is a win-win situation. Both the reduced electrical power consumed reduces the fuel consumption but also the reduced need for cooling the fan motor in the air conditioner saves fuel. The air that is cooled by the evaporator before entering the cabin is heated by the losses in the PMDC and driver. With the BLDC motor, the cooling demand is reduced and less coolant needs to be pumped by the ICE driven compressor. This saving is not investigated in this report but might be considerable. On the other hand at wintertime the excessive quick heat is more desirable.

The efficiency reached with the BLDC motor in this project, about 80 %, at rated speed and torque is slightly higher than the data from the manufacturer. Even if there may be some errors in the measurement of load power this figure is realistic. For state of the art, maximum efficiency Maxon motors have a line of motors in the same power range especially optimized for efficiency that have a maximum efficiency of up to 89 % without driver. These motors might mostly be used for non cost critical applications as the space industry. With an assumed state of the art driving circuitry efficiency at 95% the system efficiency ends at 85 %. For the cost sensitive automotive industry a high volume and low cost BLDC system efficiency, with reasonable further motor development, ends up somewhat lower than 85% at the investigated power range.

The BLDC motors of today are not optimized for high volume production as in the case with the PMDC. The cost for the additional processing power in the BLDC is today almost negligible due to low cost microprocessors with inbuilt functionality as PWM drivers and ADC´s. The development towards one chip BLDC drivers with running software on deliverance reduces the cost for programming. Toshiba recently presented a one chip sensor less BLDC driver (with built in power stage) up to 60 W output power and other manufacturers have sensor less techniques for both the PMSM and BLDC available for higher power output, although not in a one chip solution. The absence of the carbon brushes and the commutator decreases the cost and in the future the cost of PM motors should fall. The one thing endangering this development may be the cost for high flux density rotor magnets. For now, the PM material cost is decreasing but the copper cost is increasing. This benefit the PM motor compared to asynchronous motor which require copper or aluminum in the rotor.

The need for the driver in the BLDC case, as compared to a PMDC operated on/off, adds to the cost but gives crucial benefits. The microprocessor easily enables the motor system into communication with an ECU in the vehicle via the CAN bus. This adds robustness functions like error messages but also the use of feedback of speed that could be implemented as a energy saving device, for example an intelligent speed controlled pump that only pumps at the lowest speed according to system needs. The converter adds other interesting robustness functions, i.e. two phase operation during one phase failure that could be usable in critical applications like fuel- and cooling pumps.

7 Future work

An investigation of how much ICE power the 50 watts of excessive, unnecessary heat in the AC unit contributes to, via the more extensive use of the AC compressor, will furthermore reduces the fuel savings for the rebuilt actuator.

Furthermore, the motor driver importance for total efficiency could be investigated further. The BLDC driver in this project consumed in the range of a few watts but for more powerful BLDC motors these few percent of total power might be the difference for the need of extra cooling.

For the cost sensitive automotive industry a case study with a BLDC manufacturer on how to make a sensor less high volume low cost BLDC motor and driver should be implemented. If the price is reasonable more applications can be considered.

That BLDC motors can operate in harsh environments is proved by the use of BLDC motors in the Mars rovers "*Sojourner*" in 1997 and "*Spirit*" and "*Opportunity*" in 2004 [6]. Some applications might be placed close or even inside the ICE which gives a total different heat interval that needs to be investigated. Does the heat affect the BLDC system with aspects to power, efficiency and lifetime?

The mathematical model of the BLDC in Matlab/Simulink must be extended to be better comparable to the measured results over the entire speed interval. Another simulation program [33] might be more usable to simulate the transient six step commutation and/or PWM switching.

Appendix A Master Thesis outline

VOLVO

2007-03-22

Master thesis work "High efficiency actuators" (Typical 20p+20p)

To reduce fuel consumption in a vehicle everything needs to be optimised. Electrical actuators are traditionally often realised with brushed DC motors. Other efficient and robust machines can in some cases increase the efficiency, i.e. brushless DC motors.

Content in the Thesis Work:

1. Study of state of the art in the area of suitable machine types for small actuators (typical 50W to 2kW)
2. Specification and basic simulation of a typical application.
3. Efficiency measurements on an application.
4. Rebuild the application to high efficiency actuator.
5. Efficiency measurements on the high efficiency actuator
6. Evaluation of the measurements and simulations. Impact on fuel consumption.
7. Report and seminar.

The thesis work is suitable for two students who has been studying power electronics, electrical machines etc.

Application contact and more information:

Eilert Johansson
Volvo Technology
eilert.johansson@volvo.com
T. 031/3224661

Appendix B Analysis measurement error

For the used digital oscilloscope LeCroy Wavesurfer 434 some assumptions give

$$\left.\begin{aligned} E_{probe\_current/voltage} &= 1\% \\ E_{ADC\_oscilloscope} &= 1\% \end{aligned}\right\} \Rightarrow \sum E_{oscilloscope} = 2\% \,. \tag{B.1}$$

To consequently reduce common mode errors the scope were to calculate channel two subtracted from channel one to get phase to phase voltage.

The power measurement where the oscilloscope calculates the mean value of voltage times current has an additional absolute error which is due to the mean calculation that does not integrate over a discrete number of periods. This error may be estimated to 1 % as a large number of periods were sampled to gain accuracy.

For the load measurement, see section *4.2*, the axle carrying the counteracting torque from the fan should be kept as short as possible to reduce the error from the scale, i.e. a shorter axle gives a higher mass to measure. Some estimation gives the absolute error

$$\left.\begin{aligned} E_{length\_axle} &= 2\% \\ E_{scale} &= 5\% \\ E_{friction\_motor\_fittings} &= 3\% \end{aligned}\right\} \Rightarrow \sum E_{load\_measurement} = 10\% \,. \tag{B.2}$$

The absolute error for the digital tachometer is speed dependent, i.e. higher for lower speeds, but can be estimated to 0.1 % over the entire speed interval and can be neglected compared to the other absolute errors.

The load measurement error affects P_{axle} and the oscilloscope error for both reading and power calculations affects the measured power consumption, P_{in}. A worst case scenario yields

$$\frac{(100\% + 10\%)}{(100\% - 3\%)} \frac{P_{axle}}{P_{in}} = 113.4\% \frac{P_{axle}}{P_{in}} \tag{B.3}$$

$$\frac{(100\% - 10\%)}{(100\% + 3\%)} \frac{P_{axle}}{P_{in}} = 87.4\% \frac{P_{axle}}{P_{in}} \tag{B.4}$$

meaning that the BLDC measured efficiency of 80 % could be between 70 and 90 %.

Appendix C BLDC Waveforms

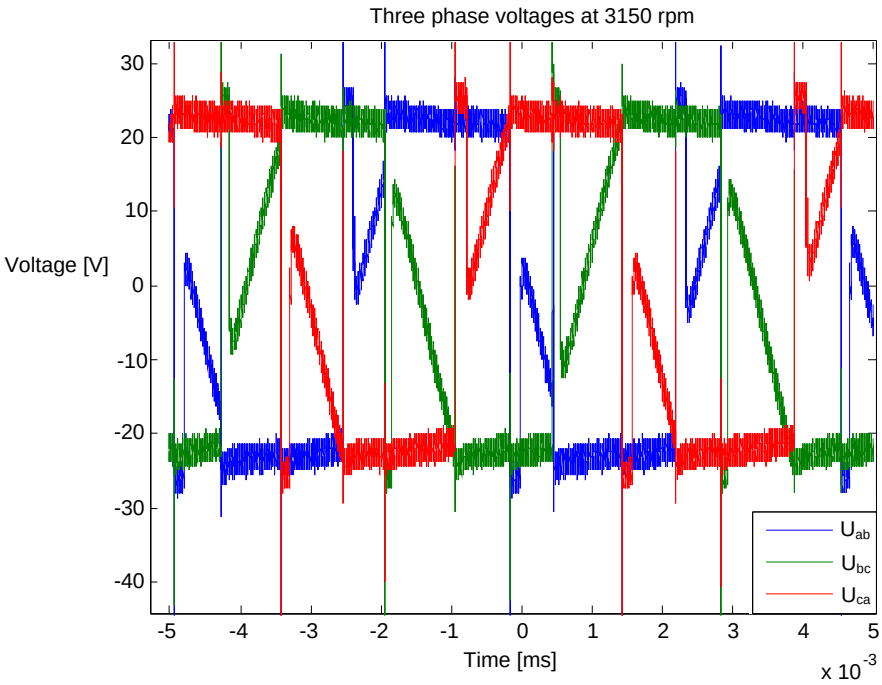

Figure C.1: Voltages at 3150 rpm

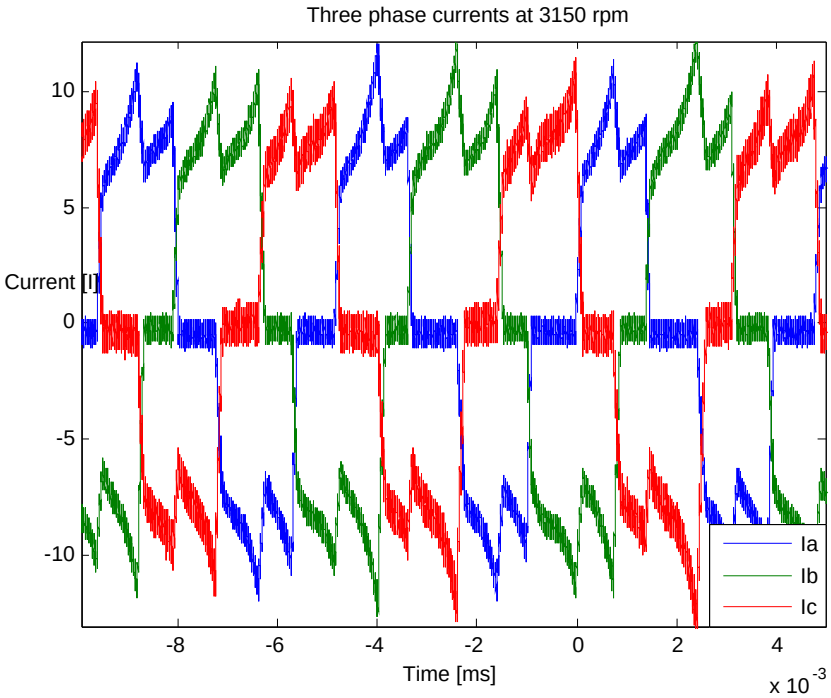

Figure C.2: Currents at 3150 rpm

References

[1] Krishnan, Ramu, *Electric motor drives: modeling, analysis and control*, Blacksburg USA, Prentice Hall, 2001, ISBN 0-13-091014-7

[2] Mohan, Ned et al, *Power Electronics: Converters, Applications and Design*, Hoboken, USA, John Wiley & Sons Inc., 2003, ISBN 0-471-42908-2

[3] Shao, Jianwen, *Direct Back EMF detection method for Sensorless Brushless DC (BLDC) Motor Drives*, Master Thesis, Blacksburg, USA, 2003

[4] Baldursson, Stefán, *BLDC Motor Modeling and Control – A Matlab®/Simulink® Implementation*, Master Thesis, Gothenburg, 2005

[5] Jons, Per Erik, *Engineering /Production development, Volvo buses*

[6] Maxon Motor, *http://www.maxonmotor.com/images/EC_max_Prospekt_e.pdf* accessed 20070905

[7] Thiringer, Torbjörn, *Department of Energy and Environment, Chalmers*

[8] Ralph, Tobias et al., Robert Bosch GMBH *US patent application nr 10483592, http://www.patentstorm.us/patents/7019479-description.html*, accessed 2007 09 12.

[9] Wikström, Rogardt, *Robert Bosch AB, Drawing PMDC motor, DPD 0130 101 616,* rogardt.wikstroem@se.bosch.com, 2007 07 19.

[10] Motion King China, *Specification 60BLDC70A-240*, 2007

[11] Leksell, Mats, *Senior Research Engineer, KTH, school of electrical engineering*

[12] Olof Nordmark, *Volvo Technology, department 6280*

[13] Lundgren, Staffan, *Volvo Technology, department 6190*

[14] Yedamale, Padmaraja, *Brushless DC (BLDC) Motor Fundamentals,* Application note AN885, Microchip Technology Inc., 2003

[15] Reston, Condit, *Sensorless BLDC Control with Back-EMF Filtering,* Application Note AN1083, Microchip, 2007

[16] R, Weiss et al, *Sensorless Regulation of a Brushless DC Motor with a C164CM,* Application Note AP1676, Infineon Technologies, 2006

[17] Infineon Technologies, *Start-Up Control Algorithm for Sensor less and Variable Load BLDC Control Using Variable Inductance Sensing Method,* Application Note AP08018, 2006

[18] Atmel, *AVR492: Brushless DC Motor Control using AT90PWM3,* Application Note 7518A-AVR-07/05, 2005

[19] Atmel, *AVR492: Sensorless Commutation of Brushless DC Motor (BLDC) using AT90PWM3 and ATAVRMC100,* Application Note 7658B-AVR-12/06, 2006

[20] Atmel, *AVR444: Sensorless control of 3-phase brushless DC motors*, Application Note 8012A-AVR-10/05, 2005

[21] Atmel, *ATAVRMC100 Hands-on Training (IAR EWAVR Version)*, Application Note Version 3_0_0-AVR-12/07/05, 2005

[22] Atmel, *ATAVRMC100: Hardware User Guide*, Application Note 7551B-AVR-02/06, 2006

[23] Atmel, *AVR434 PSC Cookbook*, Application Note 7670A-AVR-10/06, 2006

[24] Jang, G.H et al, *Optimal Commutation of a BLDC Motor by Utilizing the Symmetric Terminal Voltage*, Seoul, Korea, IEEE 0018-9464

[25] ST Microelectronics, *AN2372: Application note Low cost sinusoidal control of BLDC motors with Hall sensors using ST7FMC*, http://www.st.com/stonline/products/literature/an/12375.pdf, accessed 2007 07 04

[26] Freescale semiconductors, *Permanent magnet synchronous motor*, http://www.freescale.com/webapp/sps/site/overview.jsp?nodeId=02nQXGrrlPZL8l, accessed 2007 07 04

[27] Transmotec, http://www.transmotec.com/, accessed 2007 07 20

[28] Infineon Technologies, http://www.infineon.com/dgdl/p1609010_Brushless_DC_Motor.pdf?folderId=db3a304412b407950112b409d4b00386&fileId=db3a304412b407950112b409f53703f0, accessed 2007 07 06

[29] Educypedia encyclopedia, *Power electronics*, http://www.educypedia.be/electronics/powerelectronics.htm, accessed 2007 07 20

[30] Stegia Motors, http://www.stegia.se/motorer.php, accessed 2007 06 11

[31] Mankel, Michael, *Field Application Engineer Motor control*, International Rectifier GmbH

[32] Conner, Margery, *Permanent-magnet motors boost efficiency and power density*, EDN magazine, http://www.edn.com/article/CA6475007.html, accessed 2007 10 01

[33] Komotec, *MotorPro-BLDC software*, http://www.komotek.com/html/eng/products/pro_02.html,accessed 2007 10 06